

## General Disclaimer

### One or more of the Following Statements may affect this Document

- This document has been reproduced from the best copy furnished by the organizational source. It is being released in the interest of making available as much information as possible.
- This document may contain data, which exceeds the sheet parameters. It was furnished in this condition by the organizational source and is the best copy available.
- This document may contain tone-on-tone or color graphs, charts and/or pictures, which have been reproduced in black and white.
- This document is paginated as submitted by the original source.
- Portions of this document are not fully legible due to the historical nature of some of the material. However, it is the best reproduction available from the original submission.

NASA CR- *170433*  
ORBITING SOLAR OBSERVATORY 8  
HIGH RESOLUTION  
ULTRAVIOLET SPECTROMETER  
EXPERIMENT



(NASA-CR-170433) ORBITING SOLAR OBSERVATORY  
8 HIGH RESOLUTION ULTRAVIOLET SPECTROMETER  
EXPERIMENT Final Report (Colorado Univ.)  
85 p HC AC5/MF A01

N82-33218

CSCL 20F

Unclassified  
33556

G3/74

FINAL REPORT

Laboratory for Atmospheric and Space Physics

University of Colorado

Boulder, Colorado 80309



ORBITING SOLAR OBSERVATORY 8

HIGH RESOLUTION ULTRAVIOLET SPECTROMETER EXPERIMENT

Final Report 1980

Laboratory for Atmospheric and Space Physics  
University of Colorado  
Boulder, Colorado 80309

## TABLE OF CONTENTS

I. INTRODUCTION . . . . .	1
II. MAJOR RESULTS . . . . .	2
Oscillations	
Physical Properties of the Solar Atmosphere	
Motions in the Quiet Solar Atmosphere	
Coronal Holes	
Motions in Solar Active Regions	
Solar Flares	
Structure of Plage Regions	
Atlas	
Theoretical Studies	
Aeronomy	
OSO-8 Workshop	
III. PERFORMANCE, EVALUATION AND CALIBRATION . . . . .	8
A. PRELAUNCH	
1. Focus and Spectral Resolution	
2. Wavelength Calibration	
3. Photometric Sensitivity	
4. Scattered Light	
5. Ghosts	
B. POSTLAUNCH	
1. Focus and Spectral Resolution	
2. Wavelength Drive	
3. Photometric Sensitivity	
4. Scattered Light	
IV. DICTIONARY OF OBSERVATION TYPES . . . . .	29
1. SPACECRAFT MODES	
A. Raster Mode	
B. Center Point	
C. Offset Point	
D. Limb	
E. Sunrise/Sunset	
F. Reaction	
G. Pointing Accuracy and Stability	
2. EXPERIMENT DEFINITIONS	
A. Experiment Categories	
B. Experiment Groups	
C. Experiment Types and Descriptions	
1. Spectroheliogram	
2. Spectroheliogram Emission Maximum or Minimum	
3. Single Wavelength Monitoring	
4. Line Scan	
5. Spectrum Scan	
6. Multiple Line Scan	
7. Velocity Study (no calibration)	

8. Flare Watch	
9. Calibration with Solar Line	
10. Limb Brightening	
11. Limb Brightening -- Detailed	
12. Limb Brightening -- Multiple Line Profile	
13. Wavelength Maximum	
14. Flare Location	
15. Spectrum Range Scan	
V. THE TAPE ARCHIVE . . . . .	39

VI. REDUCTION PROGRAMS . . . . .	42
----------------------------------	----

1. SOL	
2. RDCAT.FTN	
3. SORTFD.FTN	
4. LOCATE.PRO	
5. SOLIO.FTN	
6. BLKSET.MAC	
7. GFIT.FTN	
8. GFTDAT.FTN	
8. MASSAGE	
SUBROUTINE AVG(NPT,Y,AVR,RMS)	
SUBROUTINE AVMASK(RISE,NOP,R,ANORM)	
SUBROUTINE AUTOFILE (NOP,R)	
SUBROUTINE GHOST (R,NOP,NGRATE,NGHOST,NORD,WL)	
SUBROUTINE MASK (N1,N2,RISE,NOP,R)	
SUBROUTINE POWER (NOP,R,NORD,NSTP)	
SUBROUTINE TRAN (NOP,Y)	
SUBROUTINE ZERO (X,N)1	
OPENI	
SUBROUTINE OPENI (LFILE)	
SUBROUTINE RD	
SUBROUTINE ENDR	
SUBROUTINE RDPDP	
AN EXAMPLE OF THE USE OF MASSAGE AND OPENI	
USEFUL HINTS FOR THE USE OF MASSAGE	

## I. INTRODUCTION

The success of the University of Colorado high resolution ultraviolet spectrometer aboard OSO-8 is unquestionable (see Appendix II, Bibliography). In three years of operation (over 18,000 orbits) the University of Colorado instrument performed over 29,000 experiments concerned with timely and important topics in solar physics - wave propagation, coronal heating, complex radiative transfer effects - and atmospheric physics - dynamics of NO in the earth's upper atmosphere, hydrogen balance problems. A glance at the table of contents of the Proceedings of the OSO-8 Workshop (Hansen and Schaffner, eds., 1977) indicates the seminal contribution of the University of Colorado experiment to our rapidly advancing knowledge of the sun's outer atmosphere. The project produced an excellent record of the physical state of the chromosphere and chromosphere-corona transition layer for the quiet sun; this work will provide a baseline for comparison to the phenomena of the active sun as observed from future spacecraft observatories.

Major objectives of the mission centered on studies of the structure, dynamics and energy balance of the solar corona and transition zone. These data provided boundary conditions appropriate to the testing of single- and multi-component model atmospheres and for models of active features including plages, sunspots, prominences, and flares. A systematic search was made for evidence indicating the presence of oscillations, trapped acoustic energy, and shock waves in the chromosphere and transition zone. A secondary objective was study of the structure of the earth's upper atmosphere revealed by spectral absorption features of the earth's atmosphere viewed against the solar disk.

But in many respects, the last year of operation will prove the most important, for it produced an immense store of data on the transition from solar minimum to maximum. The rapid increase during the early part of 1978 in both solar activity and instrumental sensitivity accelerated the pace of plage and sunspot observing. Observations centered about studies of the upper chromosphere and transition zone employing the high excitation lines of C IV,  $\lambda 1548$ . Continuity with the previous data was assured by continuing experiments in the chromospheric lines of Si II and Fe II. Additional data from hydrogen Ly  $\alpha$  and Si IV rounded out the plage and flare watch programs. Collaborative programs concerned with prominences and other targets of opportunity assured coverage of the full range of phenomena in this period of increasing solar activity.

This document contains a short summary of the major results obtained (Chapter II) and the instrumental methods used (Chapters III and IV and Appendix I). The data archive is discussed in Chapter V, together with methods and programs for finding experiments of interest. Chapter VI describes the use of some of the most useful data reduction programs.

## II. MAJOR RESULTS

The University of Colorado experiment aboard OSO-8 performed experiments designed to explore a very broad range of solar phenomena. In addition, aeronomy experiments were executed at spacecraft sunrise and sunset.

The University of Colorado high resolution ultraviolet spectrometer experiment aboard the Orbiting Solar Observatory 8 completed its mission after three years of operation. This instrument and the French experiment, also operated from Laboratory for Atmospheric and Space Physics (LASP), investigated solar ultraviolet phenomena that are impossible to observe from the ground. The French experiment was sponsored by the Laboratoire de Physique Stellaire et Planetaire (LPSP).

The overall goal of the CU experiment was to measure accurately the ultraviolet spectrum emitted by the solar chromosphere and the chromospheric-coronal transition region during solar activity minimum. The temperature of the solar atmosphere in the transition region abruptly jumps up to the million degree values required to drive the solar wind from the corona. Measurements made prior to OSO-8 did not have sufficient spectral resolution and speed to give an accurate spectrum and time variation. With the OSO-8 measurements, the more specific problem of the identifications of oscillations and their interpretation as wave motions in the solar chromosphere were addressed. Empirical boundary conditions were set on the theory for heating the solar corona with waves generated in the lower solar atmosphere.

The two spectrometers were the first to measure the variation of solar ultraviolet spectral lines over time scales as short as 15 seconds. The combination of the CU and LPSP spectrometers allowed simultaneous measurements of spectral variations in both the visible and ultraviolet regions of the spectrum. Known spectral properties at the visible wavelength range were verified, and the characteristics of the previously unmeasured ultraviolet variations were defined. The instrument flexibility allowed the observation of spectra of different solar regions such as the solar limb, sunspots, active regions, solar prominences, and the quiet solar disk. The basic observations of the properties of spectral lines in the 1200-2000 Å range served as a spectroscopic diagnostic for physical conditions in different solar structures. Specifically, lines emitted by CI, CII, CIV, OI, FeII, SiIII, SiIII, and HI ions have been measured. These ions exist at temperatures from 6000-200,000 K; consequently, properties of solar layers extending from the solar photosphere up into the transition region at the base of the corona can be inferred.

The following is a summary of the principal results of the University of Colorado experiment aboard OSO-8 during its three years of operation.

## Oscillations

The idea that the solar chromosphere and corona are heated by sound waves generated in the convection zone lying beneath the photosphere has been popular for many years. However, the very difficult theoretical problems associated with the generation of the sound waves and their propagation through the solar atmosphere have hindered the development of a quantitative evaluation of the role of sound waves. Strong support for the sound wave picture has been obtained from the observation of compression waves in the photosphere.

Prior to the launch of OSO-8, wave oscillations in the low chromosphere could be studied only with difficulty and with low sensitivity, while the upper chromosphere and chromosphere-corona transition were inaccessible. The LASP instrument on OSO-8 permitted the study of oscillations in these regions, and has greatly improved the sensitivity and versatility of studies in the lower chromosphere. Our most important results are the following:

Wave energy is present at all observed frequencies. Sound waves are present in the lower chromosphere with periods of 400 sec to less than 30 sec, with a broad power maximum near 300 sec. This peak seems to narrow somewhat in the brighter solar features (the network and plage regions); that is, in those features where magnetic fields are thought to dominate the chromospheric structure. From statistical analyses, all of the power in the 300 second peak has been shown to be of solar origin, as has a significant fraction of the flat noise spectrum of the solar chromospheric oscillations at frequencies away from this peak. [A previously reported peak in the power spectrum near a period of 100 seconds has been identified as an alias of the spacecraft wheel oscillation.]

The energy flux from the 300 second waves diminishes rapidly with height. The observed velocity amplitude of the waves is nearly constant through the chromosphere and possibly into the transition region. Since the density is falling rapidly with height, the resulting flux of transported energy appears to diminish rapidly with height. The observed energy flux in waves in the upper chromosphere is much too small to account for the heating of the corona, so the waves are apparently not the principal mechanism of energy transport from the photosphere to the corona. High frequency, short wavelength acoustic waves manifest themselves not as Doppler displacement of the lines, but as line broadening. If this "microturbulent" broadening is due to short wavelength acoustic waves, then the OSO-8 observations of the widths of the ultraviolet lines indicate that even these waves would not carry enough power to heat the upper chromosphere and corona.

One analysis of the phase lag of oscillations between the temperature minimum and various levels of the chromosphere and transition zone found that the apparent wave speed is supersonic (Chipman, 1978).

Apparent wave velocities between several pairs of heights in the chromosphere have been measured; the derived velocities considerably exceed the local sound velocity considerably. This implies that we are primarily looking at standing waves in a resonant cavity, rather than at simple running acoustic waves. Furthermore, the wave velocity depends on the periods of the waves observed. Another analysis of phase delays of oscillations between the two chromospheric SIII lines demonstrate an apparent upward propagation of the waves (White and Athay, 1979). Further, ground based measurements and analyses of the CNRS - LPSP data from OSO-8 seem to confirm the Chipman (1978) result. The propagation characteristics of these waves in the chromosphere and transition-zone can potentially yield a great deal of information about the structure and energetics of these layers. It is important that the observational discrepancy governing the phase delays be resolved by future spacecraft measurements. The observed nature of these waves can yield much information about the physical structure of the solar chromosphere.

#### Physical Properties of the Solar Atmosphere

The OSO-8 studies of the solar chromospheric emission lines at high spectral resolution have uncovered a number of interesting phenomena. Interpretation of the observations is in terms of a model of the temperature and pressure of the solar atmosphere as a function of height above a conventionally chosen point; the model most generally accepted is that of Vernazza, Avrett and Loeser (VAL model), and recent results are often expressed as (more or less small) variations in the parameters of the model. Some of the more important results are:

Lower Plateau Temperature - The lines of CII at 1335 Å are quite sensitive to the structure of the "plateau" in the VAL model (this is a region of almost constant temperature near 20,000 K that extends for several hundred kilometers in the upper solar atmosphere). This, together with the fact that the hydrogen spectrum is formed in a non-local manner, leads to the conclusion that the temperature of the plateau should be 16,500 K and contains 25% more material than the VAL model.

Small Scale Turbulence Measurements - The CI multiplets at 1560 Å and 1657 Å provide a useful measure of the small-scale turbulence of the atmospheres of the sun and late type stars. Because some of the doublet emission lines are blended, the theoretical analysis of them is richer (and more difficult): we have found a previously unknown spectral effect. Consider light in a certain frequency range near an emission line maximum; the overlapping part of another line (blending of the lines) will produce an increase in the number of atoms in the atmosphere able

to absorb light in this band. It may happen that the increase in absorption is so great that we can no longer "see through the atmosphere" to the region that is optimal for the formation of the lines, and consequently, the total light is reduced from the unblended case. If we now allow small scale (micro-) turbulence, the light can "leak out" in a wider band than before due to the Doppler effect; this tends to decrease the absorption in any frequency band, and consequently, the blended line emission may increase as a function of the degree of micro-turbulence. The behavior due to macro-turbulence, i.e., the addition of separate Doppler-shifted lines, would first produce an increase in the light in the blended region. Appropriate lines, then, could be used to discriminate between micro-turbulence and large scale flow in stars other than the sun.

Time series measurements by OSO-8 of transition zone lines show that this region of the solar atmosphere may not be in a steady state. The line widths and intensities undergo frequent non-periodic fluctuations. The observed temporal fluctuation in width and line position of the SiIV line suggests that MHD disturbances are likely to cause the broadening of the transition-zone lines.

Formation of the OI Lines in the Solar Chromosphere - The OI triplet at 1300 Å is primarily formed by fluorescence by Ly $\beta$ , and is sensitive to the properties of the middle and lower chromosphere. D. L. Skelton received his M.S. for his investigation of this effect.

Downflows in the Transition Region - The center to limb variation in profiles of the lines of CIV and SiIV (formed in the chromosphere-corona transition region) indicates a mean downflow of 10 km/sec in this region. At the extreme limb we find a blueshift in these (and other) lines, which can be interpreted as a mean downflow that decreases in magnitude lower in the atmosphere.

The Lyman  $\alpha$  Line Profile in the Corona - Ever since the discovery at the eclipse of March, 1970 that the Lyman  $\alpha$  line of hydrogen is the strongest coronal emission line in the solar ultraviolet spectrum, the question of the true temperature of neutral hydrogen in the corona has been unresolved. Many profile scans of this line were performed and a broadening temperature of 600,000 K derived. This temperature is remarkable in that it is considerably lower than the accepted average coronal temperature of  $1.8 \times 10^6$  K.

#### Motions in the Quiet Solar Atmosphere

The University of Colorado experiment has made studies of non-oscillatory motions: steady flows that exist in the quiet chromosphere and chromosphere-corona transition zone. The large scale flow structure of the photosphere, the supergranulation, is basically a steady flow pattern horizontal to the surface of the

sun. It is believed to be a surface manifestation of the convective motions of the solar interior with a scale size of about 30,000 km. OSO-8 observations demonstrate that this motion persists to higher levels than have been previously measured. Coordinated OSO-8 and ground-based observations have located a distinct shear layer for the supergranular motions. The flow is largely horizontal in the photosphere, but it is vertical in the chromosphere and transition region. The boundaries of this supergranulation pattern, the bright chromospheric network, have been known to participate in a steady downflow at the heights of the lower chromosphere. These downflows have been shown by OSO-8 measurements to persist well up into the chromosphere-corona transition zone. These observations have brought us closer to an understanding of where the solar atmosphere changes from a convective type of circulatory motion to the radial outflow experienced in the solar corona. As a result of these observations, the picture of the energy balance of the solar atmosphere may have to be modified. K. M. Gleason authored the M.S. thesis "A Characterization of the Gas Motions in the Solar Chromosphere-Corona Transition Region using a Statistical Analysis of Si IV  $\lambda 1393$  Profiles from OSO-8."

#### Coronal Holes

Coronal holes are now known to be sources of much of the outflowing material in the corona. Studies of the resonance lines of the SiIV at 1393 Å were undertaken to see if these steady flows may be observed in the transition zone below the corona. The SiIV line profiles observed in coronal holes have line widths about 10% greater than non-coronal hole regions, but show no observable change in line position or integrated intensity. Work on the widths and displacements of SiIV line profiles suggests non-thermal disturbances of about 40 km/sec, with an average interval between disturbances of about fifty seconds.

#### Motions in Solar Active Regions

OSO-8 observations demonstrate that steady outflows exist in the chromosphere and transition zone over sunspots. The flows are moderate (a few  $\text{Km s}^{-1}$ ) in the chromosphere, but they increase to about 20  $\text{Km s}^{-1}$  in the transition zone. These flows may be a result of the umbral flashes. Steady outflows have also been observed over an active region filament.

#### Solar Flares

A new and rather unexpected result from the OSO-8 spectrometer concerns the discovery that the flare events in the transition zone are usually accompanied by rapid downflows of up to 80  $\text{Km s}^{-1}$ . The downflow occurs at the onset of the impulsive phase of the flare, and often precedes the rise of soft X-ray intensity. These observations put severe constraints on models of solar flares. The downflow must be a manifestation, or an immediate result, of the initial flare energy release. In one

energetic event studied, the redshift was followed by a moderate blueshift near the maximum of the ultraviolet emission. Comparison of the ultraviolet observations with observations from the Mapping X-Ray Heliometer aboard OSO-8 indicate that the flare X-ray emission is due to the filling of coronal loops by heated chromospheric material.

Other observations of flares show that the transition zone of the flare may brighten in times as short as 3.5 seconds. This observation places strict constraints on flare energy release mechanisms.

Active regions have been shown to participate in frequent small flare-like brightenings of the transition zone that have little or no manifestation in the chromosphere. These brightenings are also accompanied by impulsive downflows.

### Structure of Plage Regions

The chromosphere and transition zone above active regions have areas of enhanced emission known as plages. Prior to OSO-8 models of plages indicated that the transition zone is at much higher densities than over the quiet sun. OSO-8 observations of a self-reversed C IV line profile in a plage region near the limb have clearly shown that the transition-zone material above this plage is at a much lower density than previously suggested for other plage regions.

### Atlas

An atlas of the disk center and limb spectra in the wavelength region 1690- 1870 Å has been compiled at higher spectral resolution than ever before. Line identification shows that, with the exception of some emission lines of FeII and SiIII, most of the strongest features at disk center are absorption lines due to the CO fourth positive band system. An extension of published analyses of this system to higher rotational quantum numbers is in progress. The limb spectrum differs in character from the disk center spectrum, and shows almost exclusively emission lines.

### Theoretical Studies

Investigation of OSO-8 data has resulted in several theoretical investigations. R. Roussel-Dupre authored the Ph.D. thesis entitled "The Effect of Transport Phenomena on Electron Velocity Distribution Functions and Ion Abundances in the Solar Chromosphere - Corona Transition Region," in which he considered several effects, due to the steep temperature gradients in the transition-zone, that drastically change the line emission rates. D. C. Roussel-Dupre investigated detailed line formation processes and authored the Ph.D. thesis "Stark Broadening and Redistribution Theory as Applied to the Solar Hydrogen Lyman  $\alpha$  and Lyman  $\beta$  Lines."

## Aeronomy

A number of aeronomical studies were performed during the spacecraft's life. Steven T. Massie wrote his Ph.D. thesis on the first successful absorption measurements of nitric oxide in the Earth's atmosphere. These measurements were conducted between January and August, 1977, and 30° North and South latitude. The nitric oxide absorption data, at the (1,0) delta band wavelength of 1829.41 Å, were numerically inverted to produce nitric oxide density profiles between 85 and 145 km. The major finding of the observations was that for altitudes below 95 km there is more nitric oxide at sunrise than at sunset. Between 95 and 145 km altitude, the sunrise and sunset densities are approximately equivalent.

High resolution spectral scans of the solar emission triplet of OI ( $\lambda\lambda 1302.2\text{Å}$ ,  $1304.06\text{ Å}$ ) from OSO-8 provide a means of determining the amount of atomic oxygen in the Earth's atmosphere. Variations in the equivalent width of the central absorption feature in these lines with solar zenith angle are related to the column density of oxygen atoms above the spacecraft altitude. Preliminary inversions using a simple, symmetric, exponential atmosphere suggest that previous models based on atmospheric drag and mass spectrometer measurements overestimate the quantity of atomic oxygen in the Earth's atmosphere at the time of the OSO-8 experiment. This work will form the basis of D. Perry's Ph.D. thesis.

## OSO-8 Workshop

LASP hosted an OSO-8 Workshop in November 1977 in Boulder, Colorado. The four-day workshop covered several topics of current interest including the mean solar atmosphere, magnetic structures, chromospheric activity, flares, the 300-second and related oscillations, velocity fields, and spacecraft science. The scientists involved with the LASP and LPSP programs on OSO-8 have been concentrating on these research areas and benefited from this interaction with other members of the solar physics community. Over 95 people attended the meeting, presenting 55 papers and contributing to the informative and often lively discussions that followed each set of papers. Manuscripts were collected and published in the "Proceedings of the November 7-10, 1977 OSO-8 Workshop," (edited by E. Hansen and S. Schaffner).

## III. PERFORMANCE EVALUATION AND CALIBRATION

The University of Colorado high resolution ultraviolet spectrometer experiment was designed as a solar observing facility for the collection and analysis of spectroscopic data and was placed in a 500 km circular orbit inclined 33° to the Earth's equator on June 21, 1975. This orbit was chosen to avoid exposure to the Van Allen radiation belt and to minimize the time

ORIGINAL PAGE IS  
OF POOR QUALITY

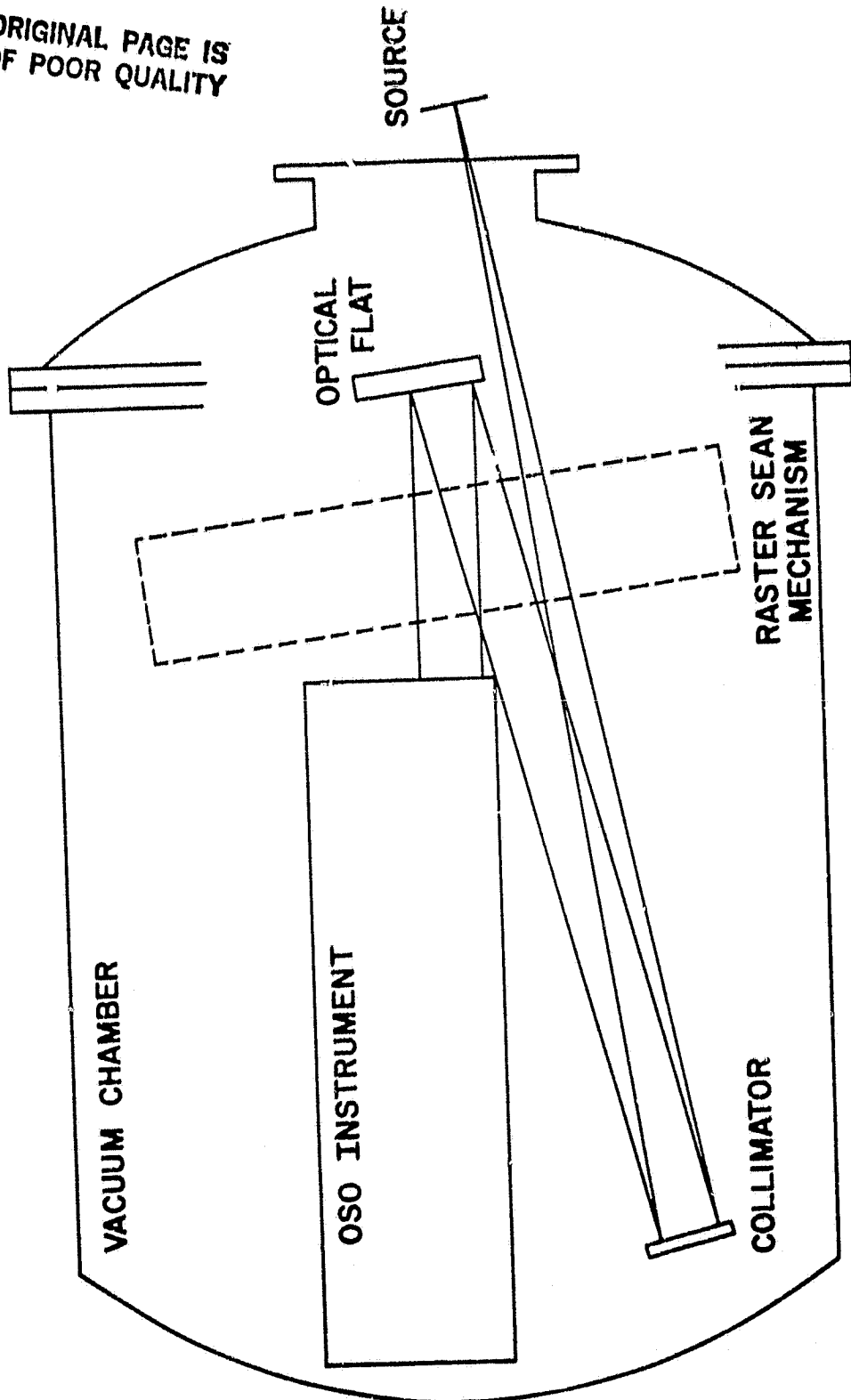


Figure 1

The wavelength drive used a sine-bar construction and is approximately linear with a nominal dispersion of 200 steps/Å. The actual dispersion was found to decrease monotonically from a value of 193.22 steps at 1213 Å to 190.92 steps/Å at 1650 Å.

### 3. Photometric Sensitivity

The instrument has a useful spectral range from approximately 1170 to 2400 Å. The end points are not sharp but are determined by the cutoffs of the filters and photocathodes. Two phototubes were used; one with a cesium iodide photocathode (G-tube) sensitive below 2300 Å and the other with a sodium chloride photocathode (T-tube) sensitive below about 1400 Å. Magnesium fluoride coatings on the telescope and spectrometer optics determine the low wavelength limit which falls sharply around 1150 Å. To permit unambiguous separation of orders in the spectrometer, four additional filters are included, with the following short wavelength cut-offs:  $\text{CaF}_2 \lambda 1260$ ,  $\text{BaF}_2 \lambda 1350$ ,  $\text{Al}_2\text{O}_3 \lambda 1440$ , and  $\text{SiO}_2 \lambda 1620$ .

The photometric response of the instrument was determined in the laboratory and is traceable to an NBS photodiode (model 543G-09-00 serial number 17195). The schedule did not allow unit level calibrations of mirror reflectance, grating efficiency, and detector efficiency and only a full instrument calibration was made. However, the final calibration is in close agreement with the product of estimated optical and detector efficiencies.

It was anticipated that the instrument would be calibrated in flight using a series of calibration rocket experiments. To achieve a desirable close similarity of in flight and laboratory calibrations, the rocket instrument to be used as a transfer was also used as the laboratory transfer. The rocket instrument consisted of a small 1/8 meter focal length Ebert-Fastie spectrometer with no collecting optics, making true irradiance measurements when observing the sun with moderate spectral resolution of  $\sim 1$  Å. In order to cross calibrate with the OSO-8 instrument, two data manipulations must be accomplished: first, a wavelength integration of the satellite data to coincide with the broad band pass of the rocket instrument and, second, the radiance measurements of the OSO instrument must be integrated over the finite source to compare with the irradiance measurements of the rocket instrument.

The prelaunch tests were carried out in a special calibration laboratory at LASP. The OSO instrument was mounted to a surface plate which served as an optical bench and included an entrance slit, 2.3 meter off-axis parabolic collimator, and a gimbal mounted optical flat to fold the beam into flight instrument (Figure 1). When the vacuum chamber was sealed, various light sources could be placed directly behind the entrance slit of the optical bench to provide collimated polychromatic beams to the instrument. The principal line sources used were a Hinteregger

gas discharge ( $O_2$ ,  $N_2$  or  $H_2$ ), mercury pen ray and r-f excited sources of  $Hg$  198 and Krypton.

The small 1/8 meter spectrometer used as the transfer standard had been flown twice as a solar rocket experiment prior to the OSO calibration. This small instrument was calibrated at the Calibration Test Equipment (CTE) facility at The Johns Hopkins University (Fastie and Kerr, 1975) before and after each rocket flight and again just prior to the final OSO calibration. The absolute accuracy of these calibrations was  $\pm 12\%$ . During the eighteen months of experience with the transfer instrument including the two rocket flights we found only minimal degradation ( $<20\%$ ).

In order to perform a calibration the entrance slit of the optical bench was aligned to the entrance slit of the OSO spectrometer. This calibration slit was  $6.4 \times 1.3 \text{ mm}^2$  and formed an image  $5.0 \times 1.0 \text{ mm}^2$  at the slit plane of the OSO spectrometer. The slit height wheel of the OSO instrument was set to the full open position but since the illumination was only over the central 5 mm, the calibrations refer only to that center portion of the photomultiplier. A map over the entire face of the PMT is discussed below. The count rate for a line source is given by:

$$\gamma(\lambda) = \frac{C(\lambda)}{\Delta t} = I(\lambda) \Omega_s A_t Q T \Delta \lambda \quad (1)$$

where  $I(g)$  is the specific intensity of the source ( $\text{photons/cm}^2 \text{ sec A ster}$ ),

$\Omega_s$  is the solid angle of the illuminated slit

$A_t$  is the telescope aperture ( $\text{cm}^2$ )

$T$  is the efficiency of the optical system (mirrors and grating)

$Q$  is the efficiency of the detector (quantum efficiency and electrical efficiency)

$\Delta \lambda$  is the bandwidth of the instrument (.01 Å second order)

$C(\lambda)$  is the count obtained in time  $\Delta t$ .

In orbit, the radiance of the sun replaces the specific intensity of the source. The 1/8 meter spectrometer transfer standard is used to determine accurately the specific intensity for either case. Since this small instrument uses no collecting optics it makes measurements of the irradiance ( $E$ ) or illuminance, related to the specific intensity by:

$$E(\lambda) = \frac{I(\lambda)ds}{F_e^2} \quad (2)$$

where  $F_c$  is the focal length of the optical bench collimator and  $ds$  is an area element of the source slit. This equation should include a  $\cos \theta$  term, where  $\theta$  is the angle between  $ds$  and the outgoing ray. In the laboratory this  $\cos \theta$  term is unity but for solar observations it is not (see Section B, 3). In the laboratory, the gimbal flat is used to map the source and it is found that the specific intensity is essentially uniform. Equation 2 therefore becomes

$$E(\lambda) = I(\lambda) \frac{L_c W_c}{F_c^2} \quad (3)$$

where  $L_c$  and  $W_c$  are the respective length and width of the calibration slit. The count rate of transfer standard is related to the illuminance by:

$$\frac{C(\lambda)}{\Delta t} = E(\lambda) A_s (QT)_{cal} \quad (4)$$

where  $A_s$  is the 1/8 meter entrance slit area and  $(QT)_{cal}$  is the efficiency in counts/photon as measured on CTE.

To compare the OSO high resolution data with the 1/8 meter data we must perform an integration over the line. This is accomplished by taking equation 1 and summing the several measurements across the line, multiplied by the sampling interval in units of the bandpass,  $\Delta\lambda$

$$R = \frac{\sum C(\lambda) \Delta\lambda s}{\Delta t \Delta\lambda} = \int I(\lambda) d\lambda A_s (QTA) \quad (5)$$

which reduces to

$$R = E(\lambda) d\lambda \frac{F_c}{F_i} \frac{w_i}{w_c} (QTA) \quad (6)$$

where  $F_c/F_i$  is the ratio of the collimator focal length to the instrument

$w_i$  is the width of the entrance slit

$w_c$  is the length of the collimator

TABLE I

$\lambda g (\text{\AA})$	Source	$\Sigma(\lambda) d\lambda$ photons/ cm <sup>2</sup> sec	$\frac{\Sigma C(\lambda)}{\Delta t}$	$\frac{\Delta \lambda_s}{\Delta \lambda}$	QTA cm <sup>2</sup>
1200	N <sub>2</sub>	2.77(6)	6.2 (4)		2.85
1216	H <sub>2</sub>	2.6 (6)	5.6 (4)		2.74
1302	O <sub>2</sub>	4.74(6)	9.5 (4)		2.55
1443	Ar	1.57(6)	1.37(4)		1.11
1494	N <sub>2</sub>	9.9 (6)	6.1 (4)		0.78
1602	Ar	3.82(6)	7.15(3)		0.24
1745 (1st)	N <sub>2</sub>	3.35(6)	1.95(4)		0.74
1745 (2nd)	N <sub>2</sub>	3.35(6)	1.75(3)		0.067
1849 (1st)	Hg	1.04(8)	3.44(5)		0.42

ORIGINAL PAGE IS  
OF POOR QUALITY

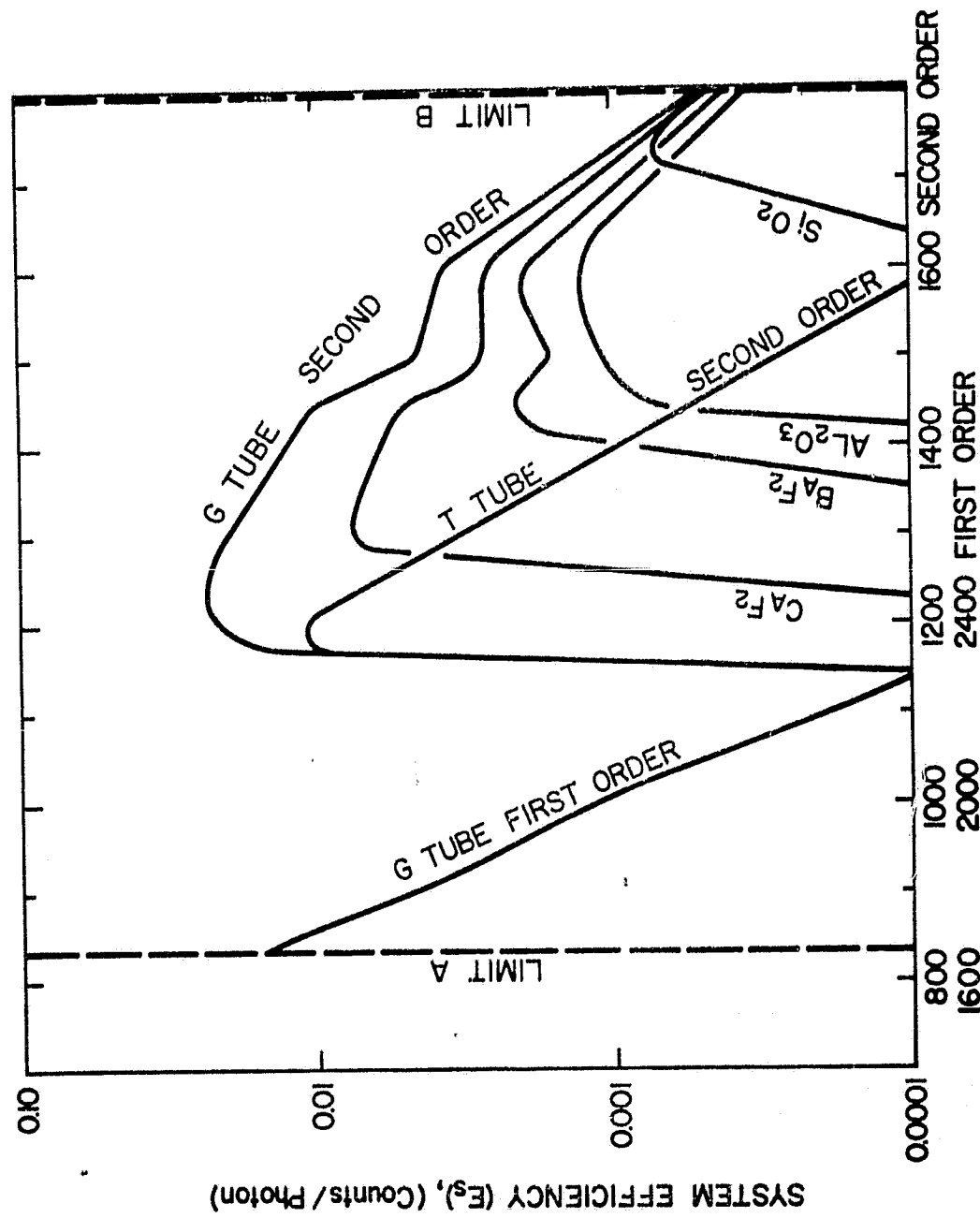


Figure 2

The geometrical factors for the laboratory calibration give:

$$\frac{F_c}{F_i} \frac{w_i}{w_c} = 7.9 \times 10^{-3}$$

A background level for both the 1/8 meter data and the satellite instrument data must be subtracted so that only the signal in the lines is compared.

The collimated beam of the laboratory source was not uniform. To obtain an average value of irradiance incident at the telescope aperture the small 1/8 meter instrument was mounted to a raster scan mechanism capable of moving the small instrument back and forth over the collimator aperture. This entire procedure was computer controlled with direct interface to the 1/8 meter data system and to the stepping motors of the raster mechanism. The computer accumulated the data, applied the calibration, and masked data points not accessible to the telescope optics.

The calibration data are given in Table 1. In addition to the calibrations shown in the table, the response of the T-phototube and the response of the G-phototube with all four filters were obtained at as many of the listed wavelengths as possible. All of the laboratory data are displayed in Figure 2. This curve shows the response of the instrument in first and second order and in all configurations of phototube with filter. The ordinate is in units of percent throughout with units of counts/photon.

The laboratory calibration met our optimistic estimates of the system throughout. The clear aperture of the telescope in the prelaunch configuration was approximately  $140 \text{ cm}^2$  and the peak efficiency (QT) of the instrument was  $\sim 2\%$ . This value is in agreement with values of 0.8 for the reflectance of each of the four mirrors (0.84 was measured by GSFC when the mirrors were coated), 0.25 for the grating efficiency and 0.20 for the detector efficiency.

The relative sensitivity as a function of position along the slit was measured as follows: the calibration slit was set perpendicular to the entrance slit of the OSO spectrometer and using the gimbal mounted flat its image was scanned from top to bottom. These measurements were made outside the vacuum chamber using Hg 2537  $\text{\AA}$  radiation. Line profiles were obtained at 2 arc min intervals across the slit. Relative sensitivities were calculated for both integrated line intensities and peak line intensity and gave essentially the same results. The slit map is shown in Figure 3. The general character of the map shows a peak efficiency near the center dropping monotonically toward the edges. Data for the map were obtained only at 2537  $\text{\AA}$  and may vary at shorter wavelengths. The photometric calibration discussed above refers to the central 5 mm of the phototube and therefore an appropriate calibration at the center of the tube

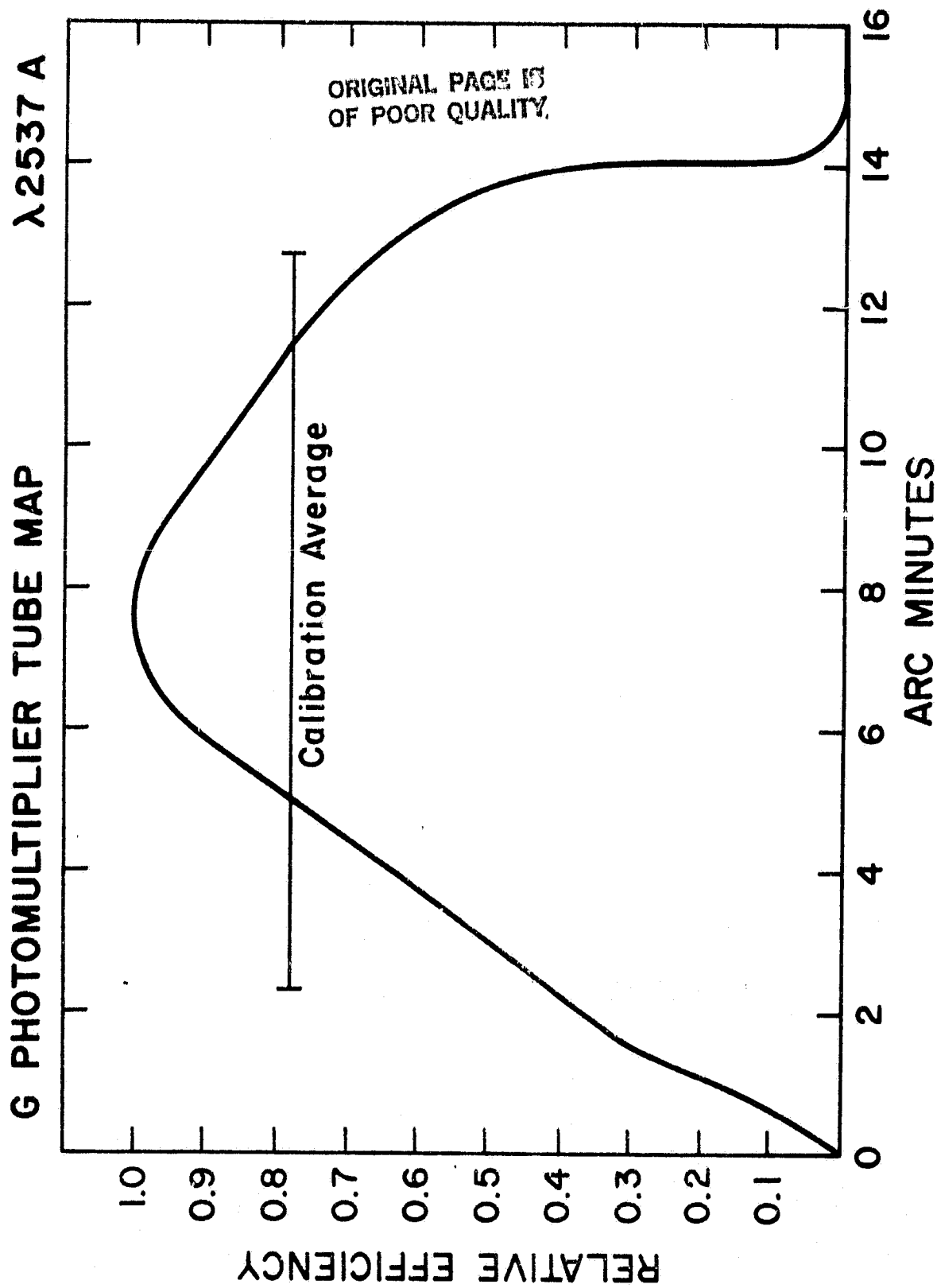


Figure 3

would raise the values in Figure 2 by approximately 25%. Likewise, a calibration for a 900 arc sec slit would lower the values by approximately 20%.

#### 4. Scattered Light

In order to make a laboratory measurement of scattered light in the OSO spectrometer a MacPherson 218 spectrometer was used as a predisperser. This instrument was modified with a special cam to move the grating accurately back and forth from the center of a strong spectral line to a position 10 Å from the line. A quantitative measure of the scattered light was obtained at 1849 Å, but a similar experiment performed at 1216 Å was hampered by a low line intensity and a drift in the source so that the data, although in qualitative agreement with the 1849 measurement, are not statistically significant for a quantitative measure.

In spite of the fact that the MacPherson 218 has a rather large amount of scattered light itself, the technique described here corrects for this scattered light in the predisperser to give an unambiguous measure of scattered light in the OSO spectrometer. A mercury pen ray lamp was used to determine scattering characteristic at 1849 Å. The OSO instrument scanned through the 1849 Å line while the predisperser was tuned on the line and again with the predisperser offset by 10 Å. The difference between these two line scans corrects for all scattered light in the instrument with the exception of scattered  $\lambda$  1849. When the predisperser is set to 1859 Å, approximately 10% of the 1849 Å line is still scattered to the OSO instrument and the difference of the OSO scans therefore only leaves  $\sim 0.9$  of the 1849 Å on band intensity. The OSO instrument is then offset to positions on each side of the 1849 Å line out as far as 250 Å separation. At each position the signal level is measured for the predisperser on and off the 1849 Å line and the difference between these two signals is the scattering of 0.9 of the 1849 Å line intensity. The ratio of this difference signal to the line intensity as measured above represents the percent of scattered light per bandpass of the instrument. As expected the scattered light levels become exceedingly small as we progress away from the central line and the statistical uncertainties of the measurements become correspondingly large. For the 1849 Å calibration the scattered light dropped rapidly to a value of  $\sim 1.5 \times 10^{-5}$  within 10 Å either side of the line, then to about  $6 \times 10^{-6}$  at 25 Å separation, and then monotonically decreased at a slower rate out to 250 Å separation.

The Lyman- $\alpha$  scattering data agreed with the 1849 Å measurement out to a 25 Å separation and beyond that point the data had large statistical uncertainties and could not be used. The scattering function of the OSO grating is most likely wavelength dependent; we assume this effect is small. The scattering function derived from 1849 Å together with a responsive curve for a solar blind G phototube implied that the scattered light level would not exceed a few percent of even the weakest solar signals

anticipated in flight and, in general, for most observations, the scattered light would be negligible.

## 5. Ghosts

The diffraction grating flown in the OSO-8 instrument (Bausch and Lomb, 3600 1/mm, 2400 Å blaze) suffered from strong pattern of Rowland Ghosts. The intensity and separation of these ghosts for a number of lines were accurately determined during the instrument calibration. Effects of the ghosts on a spectrum of arbitrary shape were numerically simulated by using a Fourier transform technique to perform the convolution of the ghost pattern with the sample spectrum. The technique is also capable of performing the deconvolution, provided that the observed spectrum segment covers a sufficiently large wavelength range. For a further discussion of the ghost removal procedure see Lites and White (1980).

## B. POSTLAUNCH

### 1. Focus and Spectral Resolution

Due to the scarcity of suitably narrow features in the solar spectrum, it proved difficult to refine the laboratory measurements after launch. Two early sets of solar observations were relevant to this problem.

The first of these was a careful measurement of the width of a line near 1300 Å tentatively identified as belonging to the Sulphur I spectrum. The width of this line had been previously measured at 0.06 Å with an echelle spectrograph of resolving power  $\sim 0.015$  Å. The width found from the OSO-8 data was 0.055 Å. This comparison, although insensitive to small departures from the measured laboratory resolution, would have revealed any deterioration more severe than about 0.03 Å F.W.H.M.

The second set of observations, made in support of an aeronomy experiment were based on an interpretation of the width of the geocoronal absorption lines in the center of the OI triplet near 1302 Å. These observations indicated that the resolution could be degraded to as much as 0.05 Å when the instrument was operated with the longest slit (900 arc seconds) and with short gate times.

### 2. Wavelength Drive

As already discussed the wavelength drive was calibrated in the laboratory using a line spectrum of molecular hydrogen in the wavelength range 1213 Å to 1650 Å. A 5th-order polynomial fit of these data was useful for the initial command and data reduction codes generated before launch. This preflight calibration was satisfactory only in the second order portion of the spectrum since no first order wavelengths were included in the analysis.

Two first order lines, 1702.04 (FeII) and 1816.93 (SiIII), were included in the initial in-flight checkout of the instrument. These lines were included with the pre-flight laboratory list and the 5th order polynomial fits were recomputed.

The polynomials used were:

$$\lambda = 1215.667 + a_1 N + a_2 N^2 + a_3 N^3 + a_4 N^4 + a_5 N^5$$
$$N = b_1 (\lambda - \lambda_0)^5 + b_2 (\lambda - \lambda_0)^2 + b_3 (\lambda - \lambda_0)^3 + b_4 (\lambda - \lambda_0)^4 + b_5 (\lambda - \lambda_0)$$

with the following  $a_i$ 's and  $b_i$ 's:

$$\begin{aligned} a_1 &= -5.17559518E-03* \\ a_2 &= -3.64082434E-10 \\ a_3 &= 1.38356650E-16 \\ a_4 &= -2.38215525E-21 \\ a_5 &= 4.71085440E-27 \end{aligned}$$

$$\begin{aligned} b_1 &= -1.93214584E+02 \\ b_2 &= -2.62571895E-03 \\ b_3 &= -2.62135302E-10 \\ b_4 &= -6.64597524E-10 \\ b_5 &= -3.11333575E-13 \end{aligned}$$

\* -03 indicates  $10^{-3}$

The reference wavelength ( $\lambda_0$ ) is that of the center of the hydrogen Lyman alpha line at 1215.667 Å. Step numbers (N) are measured away from this point, and are measured as positive in the direction toward lower wavelengths.

For use in the command generation and data reduction programs the step number at Lyman alpha was arbitrarily taken to be 160,114, so this number would be added to the step numbers N discussed above. All resulting step numbers are then positive. These polynomial fits from the initial flight data were used throughout the operational life of the instrument, and remained accurate enough for our purposes during this time period.

### 3. Photometric Sensitivity

The OSO-8 satellite was injected into orbit on June 21, 1975. The laboratory calibration of the full instrument sensitivity was completed in early June 1974. During the intervening year the instrument was integrated into the spacecraft and underwent extensive testing at Hughes Aircraft in Los Angeles. Every effort was made to control the environment of the instrument to protect it from contamination. The instrument was maintained in a clean room and all vacuum testing was conducted in oil-free pumped chambers. Upon completion of all spacecraft testing, special fixturing was set up at Hughes to attempt a photometric calibration of the instrument. In the limited time available we hoped to repeat the laboratory calibration at as many wavelengths as possible. Numerous difficulties encountered during this

testing period made it impossible to obtain a reliable calibration. A problem sending digital data from the instrument to the computer test equipment restricted the calibration to low signal levels and required the use of a small (10 arc sec) entrance slit aperture. This problem coupled with the nonuniformity across the calibration test source gave ambiguous results. The data agreed with our previous laboratory calibration. However, a slight misalignment of the instrument and test fixturing would imply that the sensitivity was down a factor of three to four.

The instrument was turned on after three days in orbit, a time period sufficiently long to allow spacecraft outgassing and prevent high voltage breakdown. Unfortunately the solar instruments acquired the sun immediately after orbit injection. This maneuver was dictated by thermal considerations but was detrimental to the instruments in that it immediately placed intense concentrated ultraviolet radiation on the secondary mirror.

This has the effect of forming polymers from material escaping from the instrument during its initial outgassing period and trapping them onto the optical surfaces. The effect is aggravated at the higher flux densities found at the surface of a Cassegranian secondary. The effect of the polymer coating is to absorb strongly at UV wavelengths.

The first experiment executed by the OSO instrument was a line scan through the Lyman- $\alpha$  line in order to reference the wavelength drive mechanism. It was immediately obvious that the instrument sensitivity was down by more than two orders of magnitude. Over the next few days the sensitivity of the instrument at Lyman- $\alpha$  recovered somewhat; this initial recovery was possibly due to the decrease in payload outgassing, primarily water vapor. After one week it was apparent that the sensitivity had decreased severely from laboratory prelaunch measurements. Between 1300  $\text{\AA}$  and 1800  $\text{\AA}$  the instrument throughput was uniformly down a factor of 15 to 20; below 1300  $\text{\AA}$ , a factor of 50.

There are many possible causes for the loss of sensitivity and it may well be that more than one loss mechanism is responsible. The single most likely source is a degradation in the optical coatings, mentioned above. John Osantowski at GSFC tested similar coatings (Al with  $\text{MgF}_2$  overcoat) contaminated with diffusion pump oil and irradiated with large amounts of hard ultraviolet radiation. The reflection of the coatings dropped sharply below 1400  $\text{\AA}$  and to a lesser extent longward of 1800  $\text{\AA}$ . Since this behavior is in qualitative agreement with the wavelength dependence of the degradation in the OSO instrument it becomes a prime candidate for the loss. The contamination problem had been anticipated and every effort was made to eliminate instrument exposure to diffusion pump oil. Unfortunately the calibration chamber at the University of Colorado and also the test chamber at GSFC (used for thermal-vacuum testing of the instrument) were oil pumped systems. Monitor mirrors failed to detect measurable contamination and we felt that the liquid

nitrogen traps of these systems were adequate. The degradation encountered is apparently caused by a combination of a small amount of contamination and the large solar flux levels. Astronomical instruments (for example OAO) may be more forgiving of contaminants due to the low light levels encountered. Our experience therefore emphasizes that for solar instruments all contaminants must be avoided, and the optical design should restrict the total ultraviolet exposure of each optical element as much as possible.

A secondary source of the loss of sensitivity may be contamination of the entrance slit. The aperture was inspected prior to launch but may have encountered dust during payload build-up and launch. Also, the slit bowl mechanism used to change the slit length may have brushed against the slit jaws during experiment set-up. The slit obscuration problem would be wavelength independent and would not account for the sharp degradation short of 1300 Å. It is also unlikely that such a loss mechanism could account for more than a factor of two decrease in sensitivity.

Calibration rocket experiments were carried out on July 28, 1975 and February 18, 1976, approximately one month and eight months respectively after OSO-8 launch. The rocket spectrometer was the same instrument used in the laboratory calibration. This small rocket instrument has no collecting optics and therefore measures the irradiance of the sun given by:

$$E(\lambda) = \frac{\int I(\lambda) \cos \theta ds}{D^2} = \bar{I}(\lambda) \Omega_\theta \quad (7)$$

where the integral is over the entire solar disc.

$I(\lambda)$  is the specific intensity or radiance of the sun

$\theta$  is the angle between the area element  $ds$  and the line of sight

$D$  is the distance to the sun (~1AU)

The irradiance is obtained directly from the rocket data by the relation:

$$\frac{C(\lambda)}{\Delta t} = E(\lambda) A_s (QT)_{Cal}$$

where

$\frac{C(\lambda)}{\Delta t}$  is the count rate of the transfer instrument

$A_s$  is the entrance slit area

$(QT)_{Cal}$  is the instrument calibration obtained at CTE facility at The Johns Hopkins University.

The transfer of calibration from the rocket instrument to the OSO instrument is similar to the laboratory transfer with one exception. In the laboratory the source had a uniform brightness and the irradiance integral (Equation 7) simplified. In the rocket experiment the sun is the common source and the radiance is not uniform.

Two techniques were used to compare the rocket (irradiance) and satellite (radiance) data sets. The first used spectroheliograms obtained by the OSO instrument to determine the contrast and limb-brightening at the desired wavelength. Analysis of these data gave the ratio between the full disc radiance and the radiance measured by the 900 arc second slit. Line profile data could then be integrated (less the background) and multiplied by the sampling interval in units of the band pass to obtain:

$$R = \sum \frac{C(\lambda)}{\Delta t} \frac{\Delta \lambda_s}{\Delta \lambda} = K \bar{I} d\lambda \Omega_{900} \text{ (QTA)} \quad (9)$$

where

$K$  is the ratio of the average radiance of the 900 arc second slit to the disc average radiance,  $\bar{I}$  ( $K = 1$ ).

$\Omega_{900}$  is the solid angle of the 900 arc second slit.

Therefore

$$R = \int E(\lambda) d\lambda \frac{K \Omega_{900}}{\Omega_{\odot}} \text{ (QTA)} \quad (10)$$

where  $E(\lambda) d\lambda$  is the line integral of the irradiance as measured by the calibration rocket instrument.  $\Omega_{\odot}$  is the solid angle of the solar disc.

The second technique involves the use of the OSO line-raster experiment. For these experiments the instrument obtains repeated spectroheliograms with a change of wavelength for each to step through the calibration line. Averaging the brightness over the sun was accomplished by summing all the elements in a raster normalized by the effective number of raster measurements that sampled the disc. The formula is:

$$\bar{C}(\lambda) = \frac{\sum C(\lambda)_{line} - \sum C(\lambda)_{wing}}{\pi/4 \text{ ab}} \quad (11)$$

where

$\Sigma C(g)_{line}$  is the sum of raster elements taken on the line.

$\Sigma C(g)_{wing}$  is the sum of raster elements taken in the far wing.

$a$  is the height of the sun in raster elements.

$b$  is the width of the sun in raster elements.

The raster difference in the numerator of Equation 11 removes the background from the line intensity and also corrects for dark count measured while the instrument is pointing off the solar limb.

The transfer of calibration for the first rocket experiment (July 1975) used the first method described above. Large rasters (128 x 128) were taken to calculate the ratio,  $K$ , of the mean solar radiance to the radiance measured by the 900 arc second slit and the 100 arc second slit placed at sun center. The OSO count rate integrated over the line was then compared with the irradiance measured by the rocket instrument to give the instrument efficiency, QTA.

This calibration was carried out for 6 wavelengths between 1216 Å and 1817 Å and the results are given in Figure 4, Curve B. Curve A is the prelaunch calibration of Figure 2 corrected for the additional vignetting of the eyeblock, which was not mounted on the telescope during laboratory tests. It is clear that the instrument sensitivity is down, slightly more than one order of magnitude at all second order wavelengths, with more serious degradation for  $\lambda > 1300$  Å. The first order sensitivity is down nearly a factor of 20.

In early August 1975 we encountered a difficulty in moving the entrance slit aperture bowl. The mechanism was set to one of the 20 arc second slits and no further attempts to move the slit were undertaken until March of 1976. When the second calibration rocket was launched on February 18, 1976, we were limited to the line-raster method of obtaining average brightness from the OSO observation. In addition, this second calibration transfer was hindered by the continuing loss of instrument sensitivity. At the time of the second rocket a complete calibration was made at only three wavelengths: 1393 Å, 1548 Å, and 1817 Å. It was possible, however, to extrapolate signal levels monitored for other wavelengths from the time of the first calibration rocket to the time of the second. These extrapolated points together with the three calibration points allow us to obtain Curve C of Figure 4. The absolute accuracy of this curve is estimated to be a factor of two longward of 1300 Å.

Several of the stronger lines observed by the OSO instrument were monitored from the time of launch. The various observations

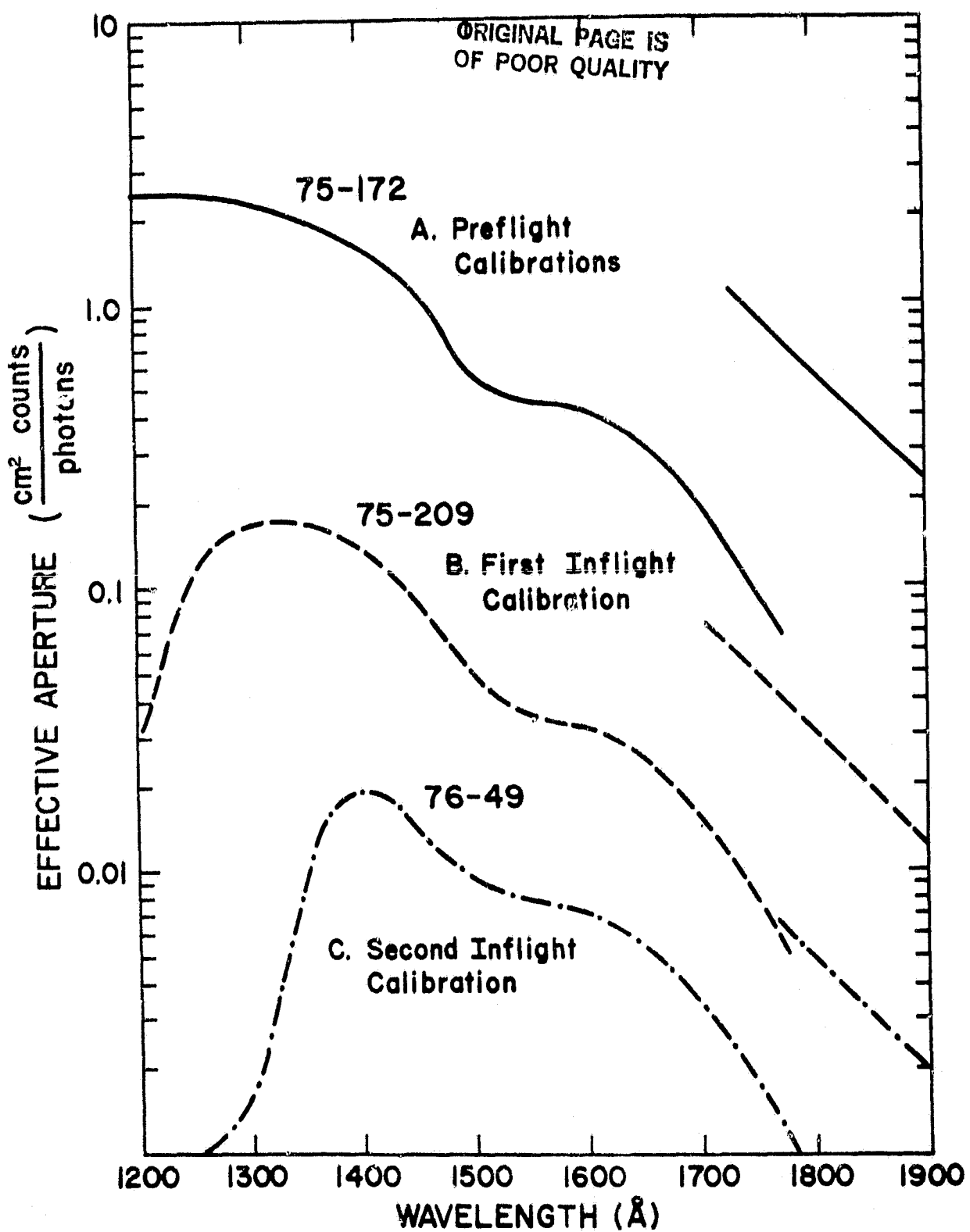


Figure 4

were normalized in units of counts per second per arc second. There is a rather wide variation in count rates due to solar activity and solar pointing coordinates. If plage and limb measurements are ignored, the signal levels tend to separate into groups according to slit size. In general the data from the slits 100 arc seconds and smaller yield signal levels approximately 50% higher than the 900 arc second data expected from the slit map calibration of Figure 3. It is apparent from these monitor curves that the instrument sensitivity was falling off with the 1/e time that monotonically increased with time. That is, the rate of decrease in sensitivity gradually became smaller until a time early in 1976, near the time of the second calibration rocket, when the instrument sensitivity appears to have stabilized. Between the middle of 1976 and the end of the OSO-8 mission in September 1978 and the instrument sensitivity seems to have decreased less than a factor of two. The large majority of experiments conducted during this period have been at wavelengths in first order. The low sensitivity in second order together with the relatively weak emission lines found below 1700 Å requires long integration times (>5 seconds) if the 20 arc second slit aperture is used.

#### 4. Scattered Light

Prelaunch measurements of the instrument scattered light were limited to two wavelengths, 1216, and 1849 Å. Those measurements predicted that the scattered light level would produce a signal to noise ratio of one for solar radiance levels of  $10^2$  photons/cm<sup>2</sup> sec Å sterad. It was anticipated that the scattered light level would be wavelength dependent since measurements of other replicas, similar to the flight grating, have shown a rather strong wavelength dependence. In spite of the unfavorable scattering characteristics of this grating, it would perform satisfactorily in the OSO-8 instrument due to the narrow bandpass used in the observations. For example, almost all central line intensities of the proposed observations exceeded  $10^5$  photons/sec cm<sup>-2</sup> Å sterad and even weak "continuum" levels would exceed  $10^3$  photons/sec cm<sup>-2</sup> Å ster.

The first observations after launch showed a strong scattered light level. It was apparent that either prelaunch measurements of scattered light were in error or that a severe change in instrument performance had occurred at, or immediately after, launch. Early attempts were made to relate the loss of sensitivity anomaly with the high level of scattered light. However, as it became clear that the instrument sensitivity loss was most likely due to an optical degradation, primarily in the telescope, a connection between the high scattered light level and low sensitivity became remote.

The prelaunch calibration tests were rechecked with no indication of severe scattered light. It should be noted, however, that the laboratory sources were all line sources with only weak continuum emissions, and no source had strong emission in the

ORIGINAL PAGE IS  
OF POOR QUALITY

spectral region 1000 to 2000 Å. Subsequent evaluation of in flight scattered light implied four characteristics:

1. The scattered light level was apparently independent of wavelength.
2. The four instrument filters affected the scattered light level in the same proportion at all wavelengths.
3. The scattered light level scaled approximately as the entrance slit length rather than as the exit slit sensitivity map obtained in prelaunch calibrations.
4. The scattered light level was decreasing with a time constant similar to the degradation in instrument response for wavelengths longer than 1400 Å.

The analysis of the scattered light employed various data sets. First, line profiles obtained by the OSO high resolution spectrometer were deconvolved to 1.2 Å spectral resolution and compared with the low resolution data of the calibration rocket experiments. These rocket experiments were known to have extreme low scattered light and the comparison gave a fairly accurate measure of the OSO scattered light at several wavelengths between 1216 Å and 1817 Å. This analysis implied the wavelength independence of the instrument scattering function. Second, sunrise and sunset data sets indicated that the extinction function of the scattered light was appropriate to a wide range of wavelengths and most likely the scattered light was approximately white as seen by the solar blind detector. Most conclusively, the OSO sensitivity curves obtained after a launch were applied to the solar UV irradiance spectrum obtained by the calibration rocket. The count rates expected using the four filters, integrated over all wavelengths, were in essential agreement with the ratios of scattered light levels obtained using the four filters.

It became evident that the most likely source of the scattered light was improper baffling of the spectrometer. The noise signal was not therefore true scattered light in the classical sense, but stray light. The Ebert optical system is so designed that there is a direct path from the entrance slit to the exit slit by way of the center of the Ebert mirror without encountering the grating. Properly placed baffles on both sides of the grating and in the center of the Ebert mirror eliminates this through path. Without proper baffling the stray light presents a serious problem and its approximate level can be estimated. Since this stray light is not transmitted by the grating, its level is not affected by the wavelength (grating angle) at which the spectrometer operates. The light is not focused at the exit slit, but can be approximated by a collimated beam. The appropriate aperture for the stray light is the area of the exit slit magnified by the square of the ratio of the focal length of the collecting telescope to the focal length of the spectrometer.

Although the efficiency of the flight grating was not measured before launch, efficiency curves exist for similar replicas. If such a grating efficiency curve is extracted from the total system sensitivity curve obtained at the time of the first calibration rocket, a suitable efficiency curve for the stray light is obtained. Again using the full disc values of the solar UV irradiance obtained by the calibration rocket instrument we expect a stray light count rate of  $\sim 5.4 \times 10^5$  counts/sec  $\text{cm}^2$  for the entire spectral range 1200 to 1850 Å using the 900 sec entrance slit. The appropriate aperture for stray light is the area of the exit slit,  $(6.4 \times 10^{-4} \text{ cm}^2)$  times the square of the ratio of the telescope focal length to the spectrometer focal length (1.8<sup>2</sup>). The expected stray light level is therefore calculated to be on the order of 10<sup>3</sup> counts per second, a result in essential agreement with observations of 1.2 to  $1.6 \times 10^3$  counts per second. This close agreement is most likely fortuitous since the estimated level includes several assumptions and is probably only accurate to a factor of two to three. The fact that the calculated level is in close agreement with the observations together with the lack of a wavelength dependence lends credence to the conclusion that the noise level is probably stray light rather than a classical scattered light.

Why was this stray light problem not detected in the pre-launch calibration and testing? An appropriate test was not conducted due to a lack of time and also the lack of a suitable source. Large slits were not available in the spectrometer and the use of the flight slits would have required a laboratory source 100 times brighter than our most intense line source to simulate the inflight stray light anomaly.

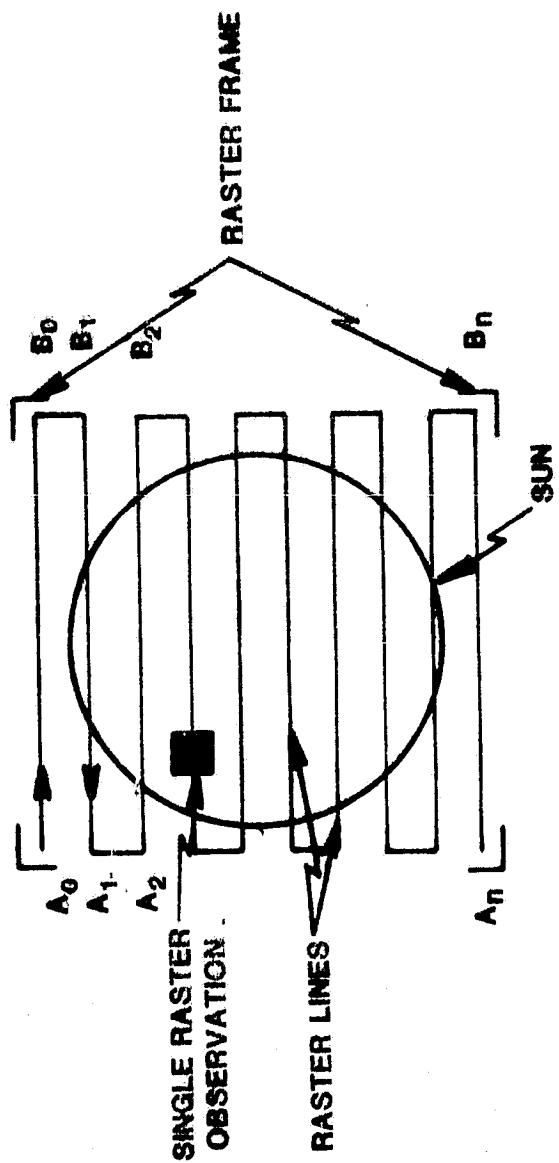
#### IV. DICTIONARY OF OBSERVATION TYPES

Because of the varied nature of these experiments, it is not convenient or useful to summarize each observing program. Instead, we have provided a catalog of final data tapes, sorted according to the kind of experiment performed. Each experiment may be adequately described by information contained in the experiment header (see Appendix V).

The Spacecraft Mode: This parameter describes the spacecraft pointing mode during the experiment. For example, it determines if the spacecraft was performing a raster of the solar disk or if it was pointing at one place on the disk.

The Experiment Type: Certain spacecraft modes were combined with sequences of operations within the CU instrument to define a limited number of "experiment types." For example, an Emission Minimum or Maximum type is a combination of a raster scan over an area of the solar surface followed by a command from the CU experiment to point at the location of maximum or minimum intensity within that area.

ORIGINAL PAGE IS  
OF POOR QUALITY



The Spacecraft Pointing Coordinates: These are spacecraft reference orthogonal coordinates of the pointing location with respect to the solar limb. The utility routines accompanying this document allow conversion of these coordinates to solar coordinates using models of solar differential rotation. In combination with a set of H photographs, they allow one to determine a solar feature within the slit or raster area.

The Experiment Category: The experiment category is a header word that describes the scientific objective and the type of solar feature under observation.

A listing and explanation of the subcategories of these parameters forms the rest of this chapter. Many other parameters in the experiment header list in the catalog (such as the wavelength of the scan or the gate time) may also be useful in selecting experiments.

## 1. SPACECRAFT MODES

The spacecraft control system can be commanded into either a raster or point mode.

### A. Raster Mode

A "raster" is used when observations are made over a rectangular area of the sun. For each of these observations the Pointed Instrument Assembly (PIA) is alternately moved along a line, left to right then right to left.

$A_0$  is the starting position for observing a line raster. Observing paths are horizontal, such as  $A_0$  to  $B_0$  and are called "raster lines." The observing path then drops vertically from  $B_0$  to  $B_1$ , and  $B_1$  to  $A_1$  is observed. The path drops vertically from  $A_1$  to  $A_2$ , and the observations are continued in this manner ( $A_n$  to  $B_n$  or  $B_n$  to  $A_n$ ).

Note that the equator of the sun will be seen in different orientations throughout the life of the experiment. On each day the orientation of the raster lines with respect to the solar equator is known to within a fraction of a degree. Rectification of raster positions the program LOCATE; see Chapter VI. This orientation is controlled by the spacecraft's attitude control system, but the amount of propellant available was limited. The time to observe (scan) one raster line (e.g.,  $A_2$  to  $B_2$ ) is called the "raster line period" either fast, (f), or slow, (s) raster requiring 5.12 sec, or 20.48 sec respectively.

The "raster frame" as shown in the figure is the entire area of observation. The time taken to observe this area on the sun is known as the "raster frame time" which varies as to the type of raster used. Raster types are defined as follows:

A large raster, designated as "R", views the full sun. The raster size (dimension) is nearly 40 arc minutes in the vertical direction and exactly 44 arc minutes in the horizontal direction. A "fine" raster scans 128 lines; a "coarse" raster scans 64 lines.

A small raster, "r", views a selected area of the sun. The raster size is approximately 2.30 arc minutes in the vertical direction and exactly 2.75 arc minutes in the horizontal direction. A "fine" raster scans 16 lines, and a "coarse" raster scans eight lines.

Individual raster modes are determined by the spacecraft (S/C) mode of operation and are:

R128f	Large, Fine, Fast Raster
R128s	Large, Fine, Slow Raster
R64f	Large, Coarse, Fast Raster
R64s	Large, Coarse, Slow Raster
r16f	Small, Fine, Fast Raster
r16s	Small, Fine, Slow Raster
r8f	Small, Coarse, Fast Raster
r8s	Small, Coarse, Slow Raster

The raster line periods and raster frame times are predetermined and cannot be varied by the experimenter. The time for each type of raster is given in Table II. The optimum gate time in the last column is the time required for the scan to sweep through a distance approximately equal to the slit length, i.e., to define a data point for a nearly square area on the sun. The exact vertical dimensions of the various rasters, defined as the distance between the top and bottom lines of the raster pattern, are also included.

#### B. Center Point

When the Pointed Instrument Assembly (PIA) is pointing at the center of the sun, the spacecraft mode is known as "center point."

#### C. Offset Point

When the PIA is pointed at any distinct position located in the 40 arc min x 44 arc min pointing range, the spacecraft mode is known as "offset point."

TABLE II

## LINE PERIOD AND FRAME TIMES

MODE	ARC SEC LINE SEPARATION	SLIT MASK LENGTH	EXACT VERTICAL DIMENSION	TIME PER LINE	TIME PER RASTER	OPTIMUM GATE TIME
						ARC SEC PER SEC
R128f	18.8 arc sec	18.8 arc sec	39.7 arc min	5.12 sec	11.0 min	470 0.04 sec
R128s	18.8	18.8	39.7	20.48	44.0	117 0.16
R64f	37.5	37.5	39.4	5.12	5.5	470 0.08
R64s	37.5	37.5	39.4	20.48	22.0	117 0.32
r16f	9.4	9.4	2.34	5.12	1.4	29 0.32
r16s	9.4	9.4	2.34	20.48	5.5	7 1.3
r8f	18.8	18.8	2.19	5.12	0.7	29 0.65
r8s	18.8	18.8	2.19	20.48	2.7	7 2.7

#### D. Limb

This is a combined mode where the spacecraft is moved from one offset point to another within a single experiment as in the Limb Brightening Experiment.

#### E. Sunrise/Sunset

These two modes were defined for convenience in experiment management. They use the spacecraft point center mode and differ from this only in that they occur as the orbit goes through the dawn/dusk transition periods.

#### F. Reaction

Reaction modes include all the above raster, point, and combined spacecraft modes. Thus, when a reaction mode experiment is defined, the specific spacecraft mode must also be included. Reaction mode experiments are used to study unpredicted solar activity.

#### G. Pointing Accuracy and Stability

Pointing was accomplished by means of fine sun sensors attached directly to the two instruments. These sensors produced error signals proportional to the X-axis and Y-axis deviations from solar center. Either the CU or the CRNS fine sensor could be used to control the spacecraft pointers. The pointing stability was  $\pm 3$  arc sec over one orbit and  $\pm 1$  arc sec over five minutes. The pointing system was capable of returning, within one orbit day, to a previously commanded offset position with an accuracy of  $\pm (3 \text{ arc sec} + 0.4 \text{ per cent of the commanded offset from sun center})$ . The pointing was slightly better than this near solar center.

In specifying an offset point position, the X- and Y- axes are divided into 2048 and 1024 parts, respectively, corresponding to 1.29 arc sec per division in the horizontal and 2.346 arc sec per division in the vertical.

### 2. EXPERIMENT DEFINITIONS

Experiments are identified by Experiment Category, Experiment Group, and Experiment Type. Experiment Categories identify the scientific objective of a specific experiment. Experiment Groups describe the spacecraft mode and set-up for an experiment. Experiment Types describe the operations of the CU instrument to obtain the desired data.

#### A. Experiment Categories

The identification of the scientific objective of an experiment is made at the time the experiment parameters are specified. This identification is useful as a key label in the cataloging

system. The following categories defined. Also listed are the corresponding computer binary values.

<u>Category</u>	<u>Bits 10-5</u>	<u>Category</u>	<u>Bits 10-5</u>
Network	000001	Limb Prominence	001100
Cell	000010	Disc Prominence	001101
Velocity	000011	Flare -- CU	001110
Average	000100	Flare -- CNRS	001111
Plage	001010	Coronal Hole	010000
Sunspot	001011	Bright Point	010001

## B. Experiment Groups

These groups are sequences of spacecraft commands commonly used by CU/CNRS. They describe the spacecraft mode and set-up for an experiment. A number of groups were defined at CU, each specifying a different command sequence. When a group is called for, the experimenter was asked to specify parameters that are unique to that experiment. As an example, a group may be named POINT. When called, this group would automatically generate the commands required to set up the spacecraft for a point mode experiment. The experimenter would be asked to supply only the experiment initiation time and the coordinates of the position to be observed.

## C. Experiment Types and Descriptions

### 1: Spectroheliogram

Observation of the variation of a single wavelength (or several wavelengths in a line profile) with time and with position on the solar disc.

The experimenter can choose to observe a single wavelength for many raster frames or to step to the next wavelength along the line profile at the end of each raster frame. The area observed and the speed of the raster is determined by the raster mode selected. The gate times are selected so that nearly square elements are observed.

This experiment can be used in any of the eight spacecraft-initiated raster modes.

### 2: Spectroheliogram Emission Maximum or Minimum

Determination of the maximum or minimum emission in the area observed by a spectroheliogram.

Junior finds the position corresponding to maximum (minimum) intensity during the first raster frame. Junior then sends an event flag signal to the Stored Command Processor (SCP) during the second raster frame. This event flag signal initiates a routine in the SCP to halt the raster on the position of interest. The next point mode experiment is then initiated.

The experiment can be used in any of the S/C-initiated raster modes.

### 3: Single Wavelength Monitoring

Repeated observation of the intensity at one wavelength at one position on the solar disc in order to monitor changes with time.

This is a point mode experiment.

### 4: Line Scan

Observation of the profile of a single line at a single position.

This line may be repeatedly scanned to observe changes or shifts in the line with time.

This is a point mode experiment.

### 5: Spectrum Scan

Observation of a large part of the solar spectrum.

The spectrum may be repeatedly observed if desired. Only about 15 Å can be scanned at the highest resolution in one orbit at a one second gate time, so a series of spectrum scans is made for large spectrum maps.

This is a point mode experiment.

### 6: Multiple Line Scan

Observation of up to eight individual line profiles at a single position.

The group of lines may be repeatedly scanned to observe changes or shifts in the lines with time. The instrument will scan across one line, then slew to the starting wavelength for the next line and scan across that line. All the lines will be sequentially scanned before the next repetition. Each of the lines may be scanned using different gate times. The number of data points per line and wavelength steps between data points ( $\Delta\lambda$ ) must be the same for each observed line profile.

This is a point mode experiment.

## 7: Velocity Study (no calibration)

This experiment is identical to the line scan experiment (type 4) except that no more than 64 data points per line profile are allowed. Up to 127 wavelength drive steps between observations may be used. The division into two experiment types is made for efficient data handling and storing.

## 8: Flare Watch

Observation of the intensities at one wavelength with position within a small raster frame.

Junior monitors these intensity values until a threshold is exceeded. The raster is halted at the position of high intensity for a point mode flare study experiment.

## 9: Calibration with Solar Line

Shifts in the wavelength with respect to the wavelength drive step number scale can be determined by scanning an emission line in the solar spectrum appearing at a known wavelength.

One of five lines may be used. Junior will scan the line, calculate the step number of the center of mass, and store the shift from the nominal center of mass step number. This shift can be added algebraically to the nominal step number for any specified wavelength. The X-coordinate in the center of mass calculation is the number of steps from the anticipated (last) value for the line center.

## 10: Limb Brightening

Observation of a line profile repeated fewer than 64 times at each preselected position on the disc or above the limb.

This line profile will have fewer than 64 wavelength points. Any set of positions may be selected to study the limb, an active region, or any other region of interest. The positions may be specified in units of 1.29 arc sec in azimuth and 2.34 arc sec in elevation within the 40 x 44 arc min field of view. Junior will issue an event flag signal when finished at one position and ready to make observations at the next position. The event-initiated routine will command the pointed instruments to the next preselected position. The event routine will then modify itself so that a different position is selected on the next event signal. The last command in the event routine will inform Junior that the routine is finished. When Junior receives this message, it will reinitiate the repeated line profile.

11: Limb Brightening -- Detailed

This experiment is identical to the Limb Brightening Experiment. The user is allowed to observe up to 1024 data points per line profile instead of up to 64. The separation into two different experiment types is done for efficient handling of the data in Boulder.

12: Limb Brightening -- Multiple Line Profile

Observation of up to eight line profiles at positions on the disc and above the limb.

Any set of positions may be selected in order to study the limb, an active region, or any other region of interest. Junior will issue an event flag signal when finished at one position and ready to make observations at the next position. The event-initiated routine will command the pointed instruments to the next preselected position. The event routine will then modify itself so that a different position is selected on the next event signal. The last command in the event routine will inform Junior that the routine is finished. When Junior receives this message, it will reinitiate the repeated multiple line profile at the new position.

The entire sequence may be repeated many times by specifying a multiple of the actual number of different solar positions to be studied. For example, if an experimenter wanted to repeat a study 5 times at 15 different solar positions, the specified number would be 75.

13: Wavelength Maximum

Observation of a single line profile at one position on the solar disc.

Junior determines the wavelength corresponding to the maximum intensity in the line profile. Junior adds or subtracts the specified wavelength correction and stores the resultant wavelength drive step number for future use.

14: Flare Location

One of the wheel experiments on OSO-I is an X-ray experiment capable of detecting flares.

When a flare occurs, the X-ray experiment sends an event signal to the SCP. The event-initiated routine issues commands to begin a large raster and to inform Junior of the flare. Junior sets up the instrument for the Flare Location Experiment and begins taking data.

Junior compares each inter :y count to a preset threshold value. When a count is found which exceeds the threshold, Junior

starts to set up the instrument for the second phase of the experiment (fine flare location) and prepares to send an event signal to the SCP. The event-initiated routine halts the large raster and starts a small raster centered about the position of the coarsely located flare.

The second phase of this experiment is the fine flare location. In the first small raster, Junior determines the brightest point within the raster frame. On the second small raster Junior sends an event signal to halt the PIA at this bright spot. The PIA remains fixed at this position for any further point mode studies. Phase II is an emission maximum experiment, type 2.

The above steps take from two to ten minutes. When the location of a flare, however, could be predicted from a planning map or from ground observations, it was not necessary to locate the flare in the large raster mode. Instead, the experiment was started in the small raster (phase II). The event routine initiated by the X-ray experiment starts a small raster about the predicted location and Junior will initiate phase II of the experiment.

#### 15: Spectrum Range Scan

The spectrum range scan experiment is similar to the spectrum scan experiment (Type 5). The differences are in the original wavelength specification, the number of wavelength positions observed, and the number of steps,  $\Delta\lambda$ , between observed points. In the original specifications, the wavelength range instead of the central  $\lambda$  is specified. Up to 32,767 wavelength steps may be observed within a single experiment. The number of repeats is restricted to 64 and the  $\Delta\lambda$  to 64. This type is useful in experiments where a large part of the spectrum is scanned in a short time. For example, a counting interval of 0.160 sec allows us to scan 90  $\text{\AA}$  of the spectrum within one orbit.

### V. THE TAPE ARCHIVE

All data collected by the University of Colorado (LASP) instrument aboard OSO-8 are contained on 103 magnetic tapes, plus one catalog tape, archived in the National Space Science Data Center. The data are sorted into groups by experiment type; the arrangement on the tapes in any one group is chronological by experiment number. An index to the almost 30,000 observing programs is contained on the catalog tape. The entire OSO-8 data record can be searched for any specific type of experiment by giving appropriate input to the program RDCAT. This program searches the catalog tapes for the particular combination of parameters desired and prints out a one line summary of each such observation. The summary of all experiments contained in Appendix VI was created by RDCAT. The reduction programs described in Chapter V are contained on another tape; of these programs, the most useful is the SOL data processing usage. This

chapter describes, in detail, how to find a particular type of experiment using the catalog tape.

All OSO-8 archive tapes are written on 7-track 800 BPI tapes as DOS images. The files can be most easily accessed through SOL, the interactive data processing language developed specifically for OSO-8 data analysis. For more concerning SOL, its implementation, and programs useful for the analysis of OSO-8 data written in SOL and in Fortran, see OSOPRG.DOC.

The data are sorted into seven categories according to experiment type (see below and Chapter IV). The experiment types in each category are:

S - EXPT. Types 1,2,10,11,12 (spectroheliograms).  
R - EXPT. Types 22,23 (spectrum range scans).  
SS - EXPT. Types 3,5,6,7,13,15,19,20 (spectrum scans).  
V - EXPT. Types 7,8,21 (velocity studies).  
LB - EXPT. Types 16,17,18 (limb experiments).  
M - EXPT. Types 4,14 (single wavelength monitoring).  
X - Miscellaneous.

This assignment of experiment types to categories reflects the reassignment of experiment types after experiment number 1039, when the instrument slit stuck; the experiment types are:

Type 1 - Spectroheliogram.  
Type 2 - Spectroheliogram emission maximum or minimum.  
Type 3 - Wavelength maximum.  
Type 4 - Single wavelength monitoring.  
Type 5 - Line scan.  
Type 6 - Spectrum scan.  
Type 7 - Multiple line scan.  
Type 8 - Velocity study.  
Type 9 - Limb finder.  
Type 10 - Flare watch.  
Type 11 - Spectroheliogram with limb offset.  
Type 12 - Emission maximum or minimum with limb offset.  
Type 13 - Wavelength maximum with limb offset.  
Type 14 - Wavelength monitoring with limb offset.  
Type 15 - Line scan with limb offset.  
Type 16 - Limb brightening.  
Type 17 - Limb brightening - detailed.  
Type 18 - Limb brightening - multiple line profile.  
Type 19 - Spectrum scan with limb offset.  
Type 20 - Multiple line scan with limb offset.  
Type 21 - Velocity study with limb offset.  
Type 22 - Spectrum range scan.  
Type 23 - Spectrum range scan with limb offset.

Further descriptive information concerning the experiment types may be found in Chapter IV.

The 103 sorted final data tapes are cataloged on the tape called FDCAT. The catalog consists of 103 SOL formatted files named after their corresponding FD-tapes. For example, FDSS03.CAT is the catalog of sorted final data tape SS-3, the catalog is designed to be used in conjunction with the program RDCAT (see OSOPRG.DOC), but may be read with the standard SOL OPENI/RD procedures. The files consist of an empty 256-integer word header and a (32 parameter) X (number of experiments on this sorted FD-tape) integer array. The 32 parameters are as follows:

1. Catalog number: 1-103.
2. Sequence number on tape.
3. Sequence number of experiment.
4. Starting wavelength of experiment times 10.
5. Ending wavelength of experiment times 10.
6. Roll angle in degrees times 10.
7. First dimensions of data array.
8. Second dimension of data array.
9. Commanded azimuth in arc minutes.
10. Commanded elevation in arc minutes.
11. Number of first logical record in experiment file.
12. Number of last logical record in experiment file.
13. Gate time in seconds.
14. Day of year at start of experiment.
15. Hour of day at start of experiment.
16. Minute of hour at start of experiment.
17. Experiment type (see above).
18. Experiment category (see below).
19. Number of wavelength drive steps between observations.
20. Number of observations of a line.
21. Duration of experiment in minutes.
22. Flag: experiment complete = 0/incomplete = 1.
23. Year, coded: 1 = 75, 2 = 76, 3 = 77, 4 = 78.
24. Number of lines observed.
25. Spacecraft (S/C) mode (see below).
26. Slit length in arc seconds.
27. Orbit numbers.
28. Minutes since sunrise at start of experiment.
29. Length of day for this orbit in minutes.
30. Day number of sunrise for this orbit.
31. GMT hour of sunrise.
32. GMT minute of sunrise.

Lists and descriptions of experiment categories and spacecraft modes may be found in the OSO-I User's Handbook, for convenient reference they are listed here.

#### Experiment Categories.

1. Network.
2. Cell.
4. Average.
10. Plage.
11. Sunspot.

12. Limb prominence.
14. Flare, CU.
15. Flare, CNRS.
16. Coronal hole.
17. Bright point.
18. Corona.
19. Limb.
20. Limb activity.
21. Filament.
22. Ratio.
23. Atlas.
24. Calibration.
33. Velocity, network.
34. Velocity, cell.
36. Velocity, average.
42. Velocity, plage.
43. Velocity, sunspot.
44. Velocity, limb prominence.
48. Velocity, coronal hole.
49. Velocity, bright spot.
50. Velocity, corona.
51. Velocity, limb.
52. Velocity, limb activity.
53. Velocity, filament.
56. Velocity, calibration.

Spacecraft modes are coded as follows:

- 0 R16S
- 1 R16F
- 2 R8S
- 3 R8F
- 4 R128S
- 5 R128F
- 6 R64S
- 7 R64F
- 8 Point Mode.
- 9 Limb Mode.
- 10 Sunrise.
- 11 Sunset.
- 39 Point Maximum.

## VI. REDUCTION PROGRAMS

The most useful program for OSO-8 data reduction is SOL, an interactive data language designed especially for the OSO-8 data. Certain primitive functions are integral parts of the language. These include opening an OSO-8 experiment, reading and displaying the header information. SOL was developed for the PDP11/20 and 11/34 computers, with interactive Tektronix graphics terminals (4006 and 4010). Appendix IV contains a complete handbook of SOL usage.

A series of other reduction programs have been written in FORTRAN IV. This section contains brief descriptions of these programs. All programs can be found on the tape OSO.PRG, written by the PDP 11/34 on 7-track, 800 bpi tapes by PIP.

## 1. SOL

All the relevant files for SOL are on the tape and are listed below. There are two command files:

SOLBLD.CMD - TKB command to build a new SOL.

SOLREASM.CMD - Command file to update any module and build a new SOL.

All sources are listed below and all objects are in SCAN.OLB, the object library. It should work on any RSX-11M system.

## 2. RDCAT.FTN

This is a Fortran program used to read the sorted final data catalog tape (FDCAT). It allows you to make a list of all files whose parameters (see DSDARC.DOC) satisfy the criteria of your choice from the FDCAT tape instead of having to search some large fraction of the 103-tape archive.

To build a working task the following files are needed:

RDCAT.FTN  
REORD.FTN  
IQSET.FTN  
DISPOS.OBJ

The program outputs a list of the names, and some other data described below, of all the files that satisfy your criteria. The entries in the list are:

SEQ# - The sequence number of the experiment.  
CAT# - The final sorted data tape catalog number.  
SQONTP - The sequence number of the tape.  
TYPE - Experiment type (see OSOARC.DOC and Chapter IV).  
MODE - Spacecraft observing mode (see OSOARC.DOC and Chapter IV).  
DAY - Day of year on which experiment started.  
HR - Minute of day on which experiment started.  
MN - Minute of day on which experiment started.  
DUR - Duration of experiment.  
START - Starting wavelength in angstroms.  
END - Ending wavelength in angstroms.  
D1,D2 - Dimensions of array: D1 is number of rows, D2 is number of columns.  
AZ,EL - Azimuth and elevation of initial pointing of experiment relative to sun center spacecraft up and right taken as positive.

GATE	- Gate time in seconds.
CAT	- Experiment category.
STPS	- Number of wavelength drive steps between observations.
NOBS	- Number of observations of line.
#LINS	- Number of spectral lines observed.
ORBIT	- The orbit number.
SLIT	- Slit length in arc seconds.

To use the program you decide what bounds on any of the 32 parameters (see OSOARC.DOC or Chapter V) will pick out the experiments of interest. The input tape, FDCAT, must be mounted on physical unit MT0: or MT1:. On output you have the choice between saving the output as a disk file or spooling the output to the lineprinter so that the disk file is deleted. (The disk file is called XXX.PRT).

The program does logical 'AND' among parameters and a logical 'OR' within one parameter. For example, to list all wavelength maximum and spectrum scan experiments that occurred in June, 1977 you would first specify parameter 17 (see OSOARC.DOC or Chapter V), and give it upper and lower bounds of 3 to get the wavelength maximum experiments. Second you would again specify parameter 17, and give it upper and lower bounds of 6 to get the spectrum scans. Then you would specify parameter 23 and give it upper and lower bounds of 3 to get the year. Finally you would specify parameter 14 and give it upper and lower bounds of 152 and 181 respectively to June of the year.

### 3. SORTFD.FTN

This is a Fortran adaptation of Dick Shine's program SORT.PRO to separate NCAR written data tape files into 7 categories, viz:

S - EXPT.TYPES 1,2,10,11,12	(spectroheliograms).
R - EXPT.TYPES 22,23	(spectrum range scans).
SS - EXPT.TYPES 3,5,6,7,13,15,19,20	(spectrum scans).
V - EXPT.TYPES 7,8,21	(velocity studies).
LB - EXPT.TYPES 16,17,18	(limb experiments).
M - EXPT.TYPES 4,14	(single wavelength monitoring).
X - Miscellaneous.	

This version takes into account changes made in experiment type classification at orbit 1039 and thus is good for all final data tapes before and after that orbit number.

To be used it needs to be linked to the BLKSET routines.

The reason for including SORTFD in the archive is so that questions as to just how files are divided up into the seven categories can be answered just by looking at the listing of the program.

#### 4. LOCATE.PRO

LOCATE is a SOL program designed to allow the user to input the name of an experiment and find the pointing coordinates of that experiment on the Hydrogen-alpha picture of his choice. The output consists of X, Y-coordinates of the spacecraft pointing both at the time of the experiment and rotated to the time of the user's choice. The coordinates are given in arc minutes, relative to the center of the solar disk and relative to both solar and terrestrial north. The output also includes the radial distance to the point of interest, the solar latitude and longitude, a warning if the convergence of the iteration to find the solar latitude was poor, and various roll angle data.

The program accesses the files LIMBS.DAT, and ROLL.DAT.

The user supplies the file name of the experiment in which he is interested. The program asks if the input is to be from tape or disk. If from disk the user may optionally input from any UIC. Thus, for example.

[200,201]A05601.FD;2  
A22106.FD

are two legitimate file names that may be used for input from disk. Only the second may be used for input from tape. The program then asks to what time (year, day, number of year, hour, and minute) the user would like the experiment time pointing rotated.

#### 5. SOLIO.FTN

This is a collection of Fortran routines to read and write SOL formatted data files. The files opened for input or output are closed with the standard "Call Close(LUN)."

To use these routines, they must be linked to the BLKSET routines; that is, the driving program, SOLIO.OBJ, and BLKSET.OBJ must be linked via the task builder.

#### 6. BLKSET.MAC

BLKSET is a Fortran callable routine to open a block access file. It is used by various programs in this package and need not concern the user. For more information see the BLKSET.MAC file.

#### 7. GFIT.FTN

Use the call: Subroutine  
GFIT(Y,F,N,TOL,NITER,AMP,BACK,XO,DEL,IOKAY,ERR,ISING,IGHOST).

This is a collection of subroutines which use a Newton-Raphson technique to fit a Gaussian to the input data.

Basic idea: The program makes an initial guess at parameters of a Gaussian that, by assumption, describes the data, Y(I). The program then creates matrices (A,B) which contain information about the residuals and the derivatives of the residuals. It then solves for the predicted changes in the Gaussian parameters (DELTX) that should give a better fit. It then makes the largest correction (step) possible. If the residuals have changed by a small enough amount (TOL), it quits.

This version ignores less than zero points, but fits greater than or equal to zero points.

Input:

Y - Array of data points to be fitted.  
N - Number of data points in Y to be fitted.  
TOL - Desired tolerance to which try to fit data. Must be within range (.1,.00001)  
NITER - Maximum number of iterations program is to take to find solution. (See output.)  
IGHOST - If equal to 1 takes instrument ghosts into account. Calling program must provide following information in COMMON/HEADER/NSPEC,XLAM,DLAM

Where:

NSPEC is spectral order 1,2,3.

XLAM is approximate wavelength.

DLAM is number of drive steps per observation point.

Output:

AMP,BACK,XO,DEL - The amplitude, background, line center, and line width calculated to best fit the data. If the program did not succeed in fitting data, returns all parameters equal to 0.  
F - Array containing fitted Gaussian, only of interest if ghosts in data.  
IOKAY - Flag.Returns:  
    IOKAY = 0 could not find solution to within TOL in number of iterations (NITER) allowed. If this flag comes up frequently check that you reset Niter before each call. Returns last values of parameters unless matrices found singular (ISING = 1).  
    IOKAY = 1 found minimum to specified tolerance.  
    IOKAY = 2 could not find residual reducing step. Usually means within  $2^{**}(-15)$  of Minimum - but not necessarily. User should check reasonableness of result in this case.  
    IOKAY = 3 could not make an adequate initial guess at parameters, N is less than 8, or maximum data. Data point is less than or equal to 10. It returns parameters equal to zero.  
ERR - Measure of error of fit. It is the sum of the residuals squared and is the quantity that is minimized. The program outputs ERR equal to sum over

greater than or equal to zero data points of  
 $(Y(I)-F(I))^{**2}/SIGMA^{**2}$   
where  $Y(I)$  are data points,  $F$  is approximating function, and  $SIGMA$  is variance of distribution of counts as a function of  $I$  (wavelength), for a poisson distribution, which is assumed,  $SIGMA$  can be approximated by

$$SIGMA(I)^{**2}=F(I).$$

ISING - Normally zero, set to one if matrices found singular, in which case usually means data are too noisy to be fitted.

NITER - Number of iterations actually taken. This means that NITER should be reset before each call.

\*\*\* Note: This means must reset Niter before each call. \*\*\*

TOL - Tolerance to which must find solution. If request is for TOL outside the acceptable range (.00001.1), it is reset to the nearest boundary point value. Otherwise it is left at its input value.

#### GFTDAT.FTN

This is a sample program that uses GFIT.FTN and SOLIO.FTN.

#### 8. MESSAGE

MESSAGE is a data processing routine designed to smooth spectrum scans, and also to correct for distortion of the line profiles taken with the OSO-8 University of Colorado spectrometer due to the Rowland ghosts. The basis for this routine is the fast Fourier transform and optimum filter technique described by Brault and White (1971). Although MESSAGE is intended for application to spectrum scans, Fourier transforms and power spectra of any data series (such as a single wavelength monitor time series, or a time series of line profile positions or intensities) may be easily extracted using this routine. The theory of the ghost deconvolution procedure is summarized by White and Lites (1979).

The computer program presented here consists of a series of stand-alone Fortran subroutines with which one can tailor a data processing scheme to fit the specific requirements of the data set. Outlined below is a brief description of each subroutine. The description, as well as the listing of the routines themselves, is given in alphabetical order. An example of the processing sequence for a typical data set is also given below.

#### SUBROUTINE AVG(NPT,Y,AVR,RMS)

This subroutine contains entry points to the routines ADAVR, TREND, and ATREND. All four subroutines are called with the same parameter set above. The purpose of the routine is to remove a mean value (with AVG) or a linear trend (with TREND) from the

data prior to any processing. The inverse operations are carried out by the routines ADAVR and ATREND, respectively.

Parameters: Y The data array  
Input: NPT The number of points to be processed in the array (number them less than or equal to external (dimension of Y))  
Output: AVG The average of the data in Y  
RMS The RMS fluctuation of the data about AVG

The array Y is returned with X the mean value or the linear trend removed (or replaced, in the case of the inverse operations).

#### SUBROUTINE AVMASK (RISE,NOP,R,ANORM)

This routine prepares the data for Fourier processing by first extending the data to a length  $2^n = L$ , where L is greater than the number of points, and  $2^{n-1}$  is less than the number of points. The integer n may not exceed 14. The data are extended with the mean value of the first and last points of the input array. Next, the routine forces a smooth transition to this mean value by applying a cosine-bell mask to each end of the data set. This masking procedure allows one to avoid problems arising from end point discontinuities (Brault and White, Astron, and Astrophys. 13, 169 (1971)). This routine also assures that the average is removed from the data before processing. The average is restored by a call to ADAVRM with the same parameters given for AVMASK.

##### Parameters:

Input: R The data array  
NOP The number of points to be processed in R  
RISE The halfwidth of the cosine-bell mask. Its effect is zero at points  $2*RISE$  and  $NOP-2*RISE$   
Output: ANORM The average value removed from the masked and extended data

#### SUBROUTINE AUTOFIL (NOP,R)

This routine computes the optimum Fourier filter, (Brault and White 1971) applies it to the previously computed Fourier transform of the data, and returns the reverse-transformed data into the array R. This routine must be preceded by a call to the

subroutine POWER, which computes the transform and the parameters for the optimum Fourier filter.

Parameters:

Input: NOP The original number of points in the array

Output: R The filtered data array

SUBROUTINE GHOST (R,NOP,NGRATE,NGHOST,NORD,WL)

This routine does the deconvolution of the grating ghost pattern from the data set. It then performs the inverse transform on the data and returns the result in the array R.

Parameters:

Input: NOP The original number of points in the data array

NGRATE The number of grating steps per data point

NGHOST The number of ghosts to be extracted (15 for first order, 8 for second order)

NORD The grating order (1 = first, 2 = second)

WL The wavelength of the center of the scan in Angstroms

Output: R The data array with ghosts removed

SUBROUTINE MASK (N1,N2,RISE,NOP,R)

This routine allows the user to apply a cosine-bell mask to an arbitrary segment of the data array R. The routine masks the data array to zero outside the range N1 to N2, so normally this routine would be preceded by a call to AVG in order to remove the mean intensity level of the scan.

Parameters:

Input: N1 The first point in the masked set. All points with index less than N1 are set to zero

N2 The last point in the masked set. All points with index greater than N1 are set to zero

RISE	The half-width of the cosine-bell mask	
NOP	The number of points in the original data string R	
R	The data string to be masked	
Output:	R	The masked data string

#### SUBROUTINE POWER (NOP,R,NORD,NSTP)

This routine computes the power spectrum of the data array, then it seeks a least-squares iterative fit to the power spectrum in order to determine parameters for the optimum Fourier filter. The signal in the original data is assumed to be approximately Gaussian in form. A call to this routine must precede any call to the routine AUTOFL. The parameters defining the optimum filter and certain characteristics of the data are printed at completion.

##### Parameters:

Input:	NOP	The number of points in the original data array
	R	The data array (usually this is masked)
	NORD	The grating order (1 = first, 2 = second)
	NSTP	Number of grating steps per data point
Output:		Transform of data array, and fit parameters are set in several internal COMMON areas in all the subroutines.

#### SUBROUTINE TRAN (NOP,Y)

This routine performs the Fourier transform of the data. It also contains an entry to the inverse transform INVTRAN (NOP,Y). The actual transform is performed by NCAR library routines that do the transformation using complex arrays. The complex Fourier components are stored in order of ascending transform domain frequency.

##### Parameters:

Input:	NOP	The number of data points in the original array
	Y	The array to be transformed
Output:	Y	The inverse transform operation returns the transformed data string in Y. All

output arrays for the forward transform  
are stored in COMMON areas in each  
subroutine.

#### SUBROUTINE ZERO (X,N)

This routine is used internally to the subroutines to set data arrays to zero.

#### OPENI

OPENI is a set of Fortran subroutines that enable the user to read OSO-8 University of Colorado experiment data files with the NCAR computing system. The package consists of four subroutines (OPENI, RD, ENDR, and RDPDP), and uses the NCAR byte manipulation routines GBYTE and SBYTE. The subroutines are used as follows.

#### SUBROUTINE OPENI (LFILE)

This subroutine searches through a PDP-11 format data tape for the file numbered LFILE. The file number is used exclusively, without the extension. If LFILE is set to zero, then the routine positions itself on the next file of the tape. The routine returns with the experiment header in the blank common area.

#### SUBROUTINE RD

This subroutine reads a data record. The record header is read, but not returned. The code could be modified for access to the record header. The data are returned in the blank common area.

#### SUBROUTINE ENDR

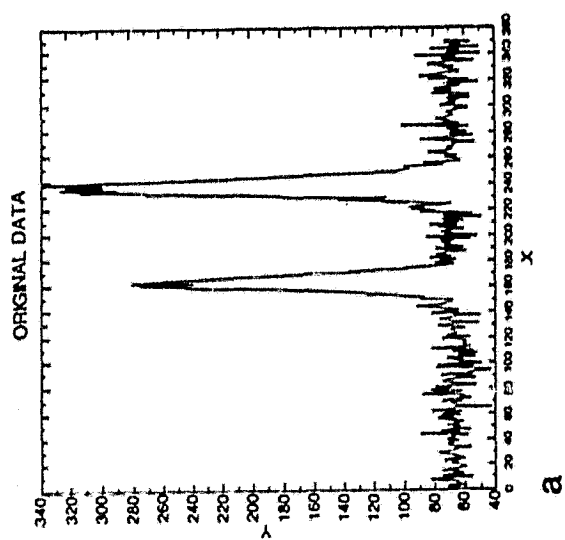
The routine ENDR positions the tape at the end of the file, ready to read the next file.

#### SUBROUTINE RDPDP

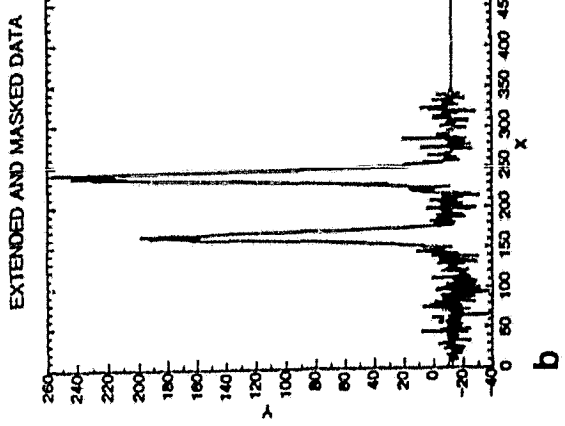
This routine is used internally to the subroutines to read the data tapes and to convert the PDP format data to Control Data 7600 format data.

#### AN EXAMPLE OF THE USE OF MASSAGE AND OPENI

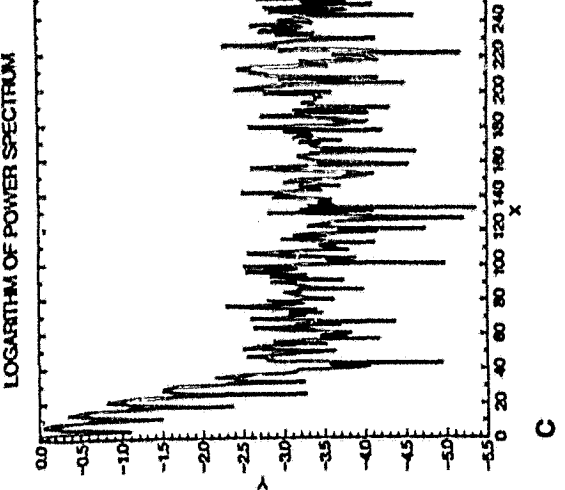
The listings of these routines are given with an illustrated example of their use on actual OSO-8 data, a scan over the C II 1335 Å lines, and the various routines are called in the main program EXAMPLE. The supplemental routine EZY is a plotting routine that was used to generate the six figures given here. The call to this routine was inserted in the subroutine POWER of MASSAGE in order to display the power spectrum. Figure a shows the original data, and Figure b shows the data, extended and



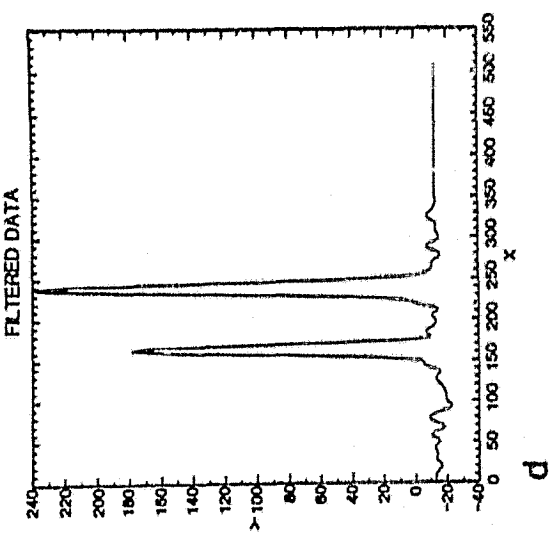
a



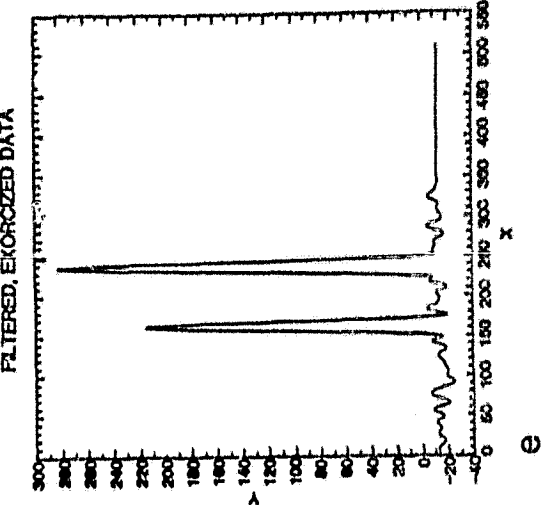
b



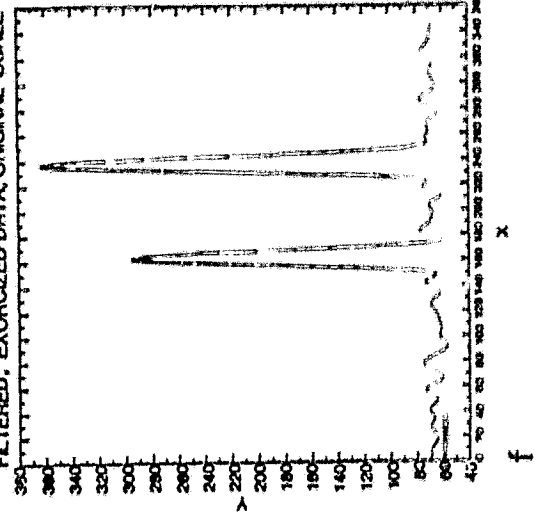
c



d



e



f

ORIGINAL PAGE IS  
OF POOR QUALITY.

masked with the mean removed, after a call to AVMASK. Figure c is the power spectrum of the resulting data string, and Figure d shows the line scan after application of the optimum filter. The filter parameters are given at the end of the listing. Figure e shows the scan after a call to GHOST, which extracts the Rowland ghosts from the data. Note that the lines are somewhat narrower and more intense. Finally, Figure f demonstrates the data with the original scaling included.

#### USEFUL HINTS FOR THE USE OF MASSAGE

The program MASSAGE cannot be considered to be a routine that will work for every sort of data encountered. Its use requires a certain amount of interaction and judgement by the user. The following suggestions may help the user in application of the program to real data.

The routine assumes that the real information in the data is roughly Gaussian in form when it derives parameters for the optimum filter. The power spectrum is accordingly fit to a parabola and a constant-level (i.e. random) noise spectrum by an iterative procedure. When the data content differ drastically from this form, for example in the case of Lorentzian line shapes, the iterative procedure may not function well. The user should always check the result of the fitting procedure to see that it is reasonable.

The masking width of the function designed to smooth discontinuities at the end of the data string should not be chosen too small so that its power spectrum does not contaminate the noise spectrum of the data. Reasonable widths are larger than, or on the order of, the narrowest spectral features of the data.

Normally, the ghost extraction routine uses 15 ghosts in first order, and 8 ghosts in second order. If the scan range is short, the ghost deconvolution for the ghosts most remote from the center of the ghost pattern can fold back into the data. Either the range of the scan can be artificially extended to a larger scan length, or the routine GHOST could be modified to extract fewer ghosts.

## APPENDICES

I. Instrument Papers\*

II. Bibliography

III. Slit Malfunction

- A. SLIT MECHANISM DESCRIPTION
- B. CHRONOLOGY OF PROBLEMS AND SOLUTIONS
- C. SLIT TESTS AND PROCEDURES
- D. CONCLUSIONS

IV. SOL Manual\*

V. Contents of Words in Experiment and Record Headers

VI. Summary Listing of Experiments Performed\*

VII. Sorted Final Data Tapes: Contents, Range and Catalog Numbers

\*Documents on file at the National Space Science Data Center.

## Appendix II: Bibliography

### OSCILLATIONS

Athay, R. G., "Chromospheric Motions Observed by the University of Colorado Experiment on OSO-8," *Proceedings of Erice Summer School in Solar Physics*, 1976.

Athay, R. G. and O. R. White, "Power Spectrum Analysis of Time Series in Positions and Intensities of Solar EUV Lines Observed with OSO-8," *IAU Colloquium 43*, 1977.

Athay, R. G. and O. R. White, "Chromospheric and Coronal Heating by Sound Waves," *Astrophys. J.* 226, 1135, 1978.

Athay, R. G. and O. R. White, 1979. "Chromospheric Oscillations Observed with OSO-8. II: Average Power Spectra for Si II," *Astrophys. J. Supplements*; March, 1979.

Athay, R. G., and O. R. White, "Chromospheric Oscillations Observed with OSO-8. IV: Power and Phase Spectra for CIV," *Astrophys. J.*, 229, 1147, 1979.

Athay, R. G., O. R. White, E. C. Bruner, Jr., E. G. Chipman, B. W. Lites, R. A. Shine, and F. Q. Orrall, "Short Period Chromospheric Oscillations Observed with OSO-8," presented at the Solar Physics Division of the 148th meeting of the American Astronomical Society (Haverford, PA), B.A.A.S. 8, 312, 1976.

Bruner, Jr., E. C., and E. G. Chipman, "Doppler Widths of Solar Chromospheric Emission Lines," presented at the 145th Meeting of the American Astronomical Society (Bloomington, Indiana), B.A.A.S., 7, 225, 1975.

Bruner, Jr., E. C., E. G. Chipman, R. A. Shine, B. W. Lites, G. J. Rottman, F. Q. Orrall, R. G. Athay, and O. R. White, "Periodic Fluctuations in the Solar Transition Zone," presented at the Solar Physics Division of the 148th meeting of the American Astronomical Society (Haverford, PA), B.A.A.S., 8, 313, 1976.

Chipman, E. G., "Chromospheric Oscillations Observed in the Line C II  $\lambda 1336$  with OSO-8," *Solar Physics*, 55, 277, 1977.

Chipman, E. G., "OSO-8 Observations of Upward Wave Propagation in the Chromosphere," presented at the 150th Meeting of the American Astronomical Society, (Atlanta, GA), B.A.A.S., 9, 323, 1977.

Chipman, E. G., "Velocity Effects in the Profiles of Self-Reversed Emission Lines," presented at the 149th Meeting of the American Astronomical Society, (Honolulu, HI), B.A.A.S., 8, 518, 1977.

Chipman, E. G., E. C. Bruner, Jr., R. A. Shine, B. W. Lites, G. J. Rottman, F. Q. Orrall, O. R. White, and R. G. Athay, "Velocities in the Solar Chromosphere Observed in the C II 1336 Line," presented at the Solar Physics Division of the 148th meeting of the American Astronomical Society (Haverford, PA), B.A.A.S., 8, 312, 1976.

Chipman, E. G., E. C. Bruner, Jr., R. A. Shine, B. W. Lites, G. J. Rottman, R. G. Athay, and O. R. White, "Preliminary Results from the Orbiting Solar Observatory 8: Velocities in the Solar Chromosphere Observed in the Si II 1816 Line," Astrophys. J. 210, L103-106, 1976.

Chipman, E. G., E. C. Bruner, Jr., R. A. Shine, B. W. Lites, G. J. Rottman, O. R. White and R. G. Athay, "Velocities in the Solar Chromosphere Observed in the Si II  $\lambda$ 1816 Line," presented at the 147th meeting of the American Astronomical Society, (Chicago, Illinois), B.A.A.S., 7, 522, 1975.

Chipman, E. G., E. C. Bruner, Jr., R. A. Shine, B. W. Lites, G. J. Rottman, R. G. Athay, and O. R. White, "Preliminary Results from the Orbiting Solar Observatory 8: Velocities in the Solar Chromosphere Observed in the S II 1816 Line," Astrophys. J., 210, 103, 1976.

Illing, R. M. E., "The 300 Second Oscillation in Si II 1817: Observed Impulse Response Function," B.A.A.S., 10, 416, 1978.

Illing, R. M. E. and B. W. Lites, "Frequency Shift of Solar Oscillations in a Flaring Region," B.A.A.S., 11, 398, 1979.

Lites, B. W., "Transition Zone Observations of Rapid Flare Events as Observed by OSO-8," submitted to Solar Physics.

Lites, B. W. and E. C. Bruner, Jr., "Transient Brightenings in Transition Zone Lines," presented at the 150th meetings of the American Astronomical Society (Atlanta, GA), B.A.A.S., 9, 323, 1977.

Lites, B. W., E. C. Bruner, Jr., and C. J. Wolfson, "OSO-8 Observations of the Impulsive Phase of Solar Flares in the Transition Zone and Corona," Solar Physics, in press.

Lites, B. W., E. C. Bruner, Jr., E. G. Chipman, R. A. Shine, G. J. Rottman, O. R. White, and R. G. Athay, "Preliminary Results from the Orbiting Solar Observatory 8: Persistent Velocity Fields in the Chromosphere and Transition Region," Astrophys. J. 210, L111-L113, 1976.

Lites, B. W., and Chipman, E. G., "The Vertical Propagation of Waves in the Solar Atmosphere: I. Observation of Phase Delays," Astrophys. J., 231, 570, 1977.

White, O. R., "High Resolution Observations of Solar Velocity Fields from Spacecraft and Rockets Using Spectroscopic Methods," Proceedings of the Nice IAU Colloquium 36, 1976.

White, O. R., "A Summary to Scientific Results from the Sail Experiments of OSO-8 During the First Year of Operation," A LASP publication.

White, O. R. and Athay, R. G., "Phase Differences Between Intensity and Doppler Shift and Between Two EUV Emission Lines of Si II for 300 Seconds and 95 Second Chromospheric Oscillations," IAU Colloquium 43, 1977.

White, O. R., and R. G. Athay, "Chromospheric Oscillations Observed with OSO-8. I: Basic Measurements and Analytical Methods," Astrophys. J. Supplements; March, 1979.

White, O. R., and R. G. Athay, "Chromospheric Oscillations Observed with OSO-8. III: Average Phase Spectra for Si II," Astrophys. J. Supplements; March, 1979.

#### PHYSICAL PROPERTIES

Francis, M. H., and R. Roussel-Dupré, "The Si IV  $\lambda$ 1393 Line in a Coronal Hole Compared to the Quiet Sun from OSO-8 Observations," Solar Physics, 53, 465, 1977.

Hansen, E. R., S. H. Schaffner, R. A. Shine, and F. Q. Orrall, "Solar Prominence Line Profiles Observed in the Ultraviolet from OSO-8," presented at the 150th Meeting of the American Astronomical Society, Atlanta, Georgia, B.A.A.S., 9, 314, 1977.

Illing, R. M. E., G. D. Toot, and R. A. Shine, "OSO-8 Observations of Velocity Shifts at the Solar Limb", in preparation.

Lites, B. W. and R. A. Shine, "Analysis of OSO-8 Measurements of the Center-to-Limb Behavior of Solar C II Line Profiles," presented at the 149th Meeting of the American Astronomical Society, Honolulu, B.A.A.S., 8, 501, 1977.

Lites, B. W., R. A. Shine, and E. G. Chipman, "Line Formation in the Solar Chromosphere: I. The C II Resonance Lines Observed with OSO-8," Astrophys. J., 222, 333, 1978.

Lites, B. W. and J. W. Cook, "A Semi-empirical Model of the Upper Flare Chromosphere," Astrophys. J., 228, 598, 1979.

November, L. J., J. Toomre, K. B. Gebbie, and G. W. Simon, "The Height Variation of Supergranular Velocity Fields Determined from Simultaneous OSO-8 Satellite and Ground-based Observations," Astrophys. J., 227, 600, 1979.

November, L. J., "Mesogranulation and Supergranulation in the Sun," Ph.D. Thesis, University of Colorado at Boulder, 1980.

Rottman, G. J., C. W. Hord, and E. C. Bruner, Jr., "High Resolution Profiles of the Solar 1304 Å Triplet, presented at the 1975 Fall Annual Meeting of the American Geophysical Union, (San Francisco, CA) December 10, 1975.

Roussel-Dupré, D. C., "Stark Broadening and Redistribution Theory as Applied to the Solar Hydrogen Lyman  $\alpha$  and Lyman  $\beta$  Lines," Ph.D. Thesis, University of Colorado at Boulder, 1979.

Roussel-Dupré, R., "The Effect of Transport Phenomena on Electron Velocity Distribution Functions and Ion Abundances in the Solar Chromosphere-Corona Transition Region," Ph.D. Thesis, University of Colorado at Boulder, 1979.

Roussel-Dupré, D., R. A. Shine, E. G. Chipman, E. C. Bruner, Jr., B. W. Lites, G. J. Rottman, F. Q. Orrall, R. G. Athay, and O. R. White, "OSO-8 Observations of Mean Vertical Motions in the Solar Transition Region," presented at the Solar Physics Division of the 148th meeting of the American Astronomical Society (Haverford, PA) B.A.A.S., 8, 312, 1976.

Shine, R. A. and B. W. Lites, "Center-to-Limb Profiles and Spatial Variations of Si II and Fe II Lines in the Solar EUV," AAS Meeting, (Atlanta, GA), B.A.A.S., 9, 325, 1977.

Shine, R. A., B. W. Lites and E. G. Chipman, "Overlapping Emission Peaks in the Solar C I Multiplets at  $\lambda$ 1560 and  $\lambda$ 1657," Ap. J., 224, 247, 1978.

Shine, R. A., B. W. Lites, E. G. Chipman, D. Roussel-Dupré, E. C. Bruner, Jr., G. J. Rottman, F. Q. Orrall, R. G. Athay, and O. R. White, "Model Calculations of Chromospheric Lines Observed by OSO-8," presented at the Solar Physics Division of the 148th meeting of the American Astronomical Society (Haverford, PA) B.A.A.S., 8, 331, 1976.

Shine, R. A., D. Roussel-Dupré, E. C. Bruner, Jr., E. G. Chipman, B. W. Lites, G. J. Rottman, R. G. Athay and O. R. White, "OSO-8 Observations of Optically Thin Lines," presented at the 147th meeting of the American Astronomical Society (Chicago, IL), B.A.A.S., 7, 552, 1975.

Shine, R. A., D. Roussel-Dupré, E. C. Bruner, Jr., E. G. Chipman, B. W. Lites, G. J. Rottman, R. G. Athay, and O. R. White, "Preliminary Results from the Orbiting Solar Observatory 8: Observations of Optically Thin Lines," Astrophys. J. 210, L106-L110, 1976.

Skelton, D. B., "The Observation and Analysis of the UV Emission of O I in the Solar Chromosphere," Thesis, Laboratory for Atmospheric and Space Physics, University of Colorado at Boulder, Boulder, Colorado 80309.

Skelton, D. L. and R. A. Shine, "Formation of the Solar O I Lines at 1304 and 1355," presented at the 150th Meeting of the American Astronomical Society, (Atlanta, GA), B.A.A.S., 9, 325, 1977.

Toot, G. D., R. M. E. Illing, "Extreme Limb Blue-Shifts of SiIII," B.A.A.S., 11, 411, 1979.

White, O. R., "A Summary of New Observations of the Chromospheric-Coronal Transition Region from OSO-8," presented at the Solar Physics Division of the 148th meeting of the American Astronomical Society (Haverford, PA), June, 1976.

## DYNAMICS

Billings, D. E., R. Roussel-Dupré, and M. H. Francis, "Dynamical Implications of Si IV Line Profiles from OSO-8 Observations," Solar Physics, 55, 287, 1977.

Bruner, E. C., Jr., "Dynamics of the Solar Transition Zone," Astrophys. J. 226, 1140, 1978.

Bruner, E. C. Jr., and R. W. P. McWhirter, "The Observation and Interpretation of the Profile of C IV  $\lambda$ 1548 Emitted from a Quiet Region of the Sun," Astrophys. J., 231, 557, 1979.

Bruner, Jr., E. C., E. G. Chipman, B. W. Lites, G. J. Rottman, R. A. Shine, R. G. Athay, and O. R. White, "High Resolution Spectroscopy from Orbiting Solar Observatory VIII: Transition Zone Dynamics Over a Sunspot," presented at the 147th meeting of the American Astronomical Society (Chicago, IL), B.A.A.S., 7, 522, 1975.

Bruner, Jr., E. C., E. G. Chipman, B. W. Lites, G. J. Rottman, R. A. Shine, R. G. Athay, and O. R. White, "Preliminary Results from the Orbiting Solar Observatory 8: Transition-Zone Dynamics Over a Sunspot," Astrophys. J. 210, L97-L101, 1976.

Bruner, E. C., Jr. and B. W. Lites, "Transient Brightenings in Transition Zone Lines," presented at the 150th Meeting of the American Astronomical Society (Atlanta, GA), B.A.A.S., 9, 323, 1977.

Bruner, E.C., Jr. and B. W. Lites, "Mass Motions in Impulsive Flarelike Brightenings as Observed by OSO-8," Astrophys. J., 228, 322, 1979.

Chipman, E.G., "OSO-8 Observations of Wave Propagation in the Solar Chromosphere and Transition Region," Astrophys. J., 224, 1978.

Gleason, K. M., "A Characterization of the Gas Motions in the Solar Chromosphere-Corona Transition Zone Using a Statistical Analysis of Si IV  $\lambda 1393$  Profiles from OSO-8," M.S. Thesis, Department of Astro-Geophysics, Graduate School, University of Colorado at Boulder, Boulder, Colorado, 1978.

Lites, B. W., "Steady Flows in the Chromosphere and Transition Zone above Active Regions as Observed by OSO-8," Solar Physics, in press.

Lites, B. W., E. C. Bruner, Jr., E. G. Chipman, R. A. Shine, G. J. Rottman, O. R. White, and R. G. Athay, "Persistent Velocity Fields in the Middle Chromosphere," presented at the 147th meeting of the American Astronomical Society (Chicago, IL), B.A.A.S., 7, 522, 1975.

Lites, B. W., E. R. Hansen, R. A. Shine, E. G. Chipman, E. C. Bruner, Jr., F. Q. Orrall, R. G. Athay, O. R. White, and G. J. Rottman, "Repetitive Brightenings in Active Region Transition Zone Lines as Observed with OSO-8," presented at the Solar Physics Division of the 148th meeting of the American Astronomical Society (Haverford, PA), B.A.A.S., 8, 331, 1976.

Lites, B. W. and E. R. Hansen, "Ultraviolet Brightenings in Active Regions as Observed from OSO-8," Solar Physics, 55, 347, 1977.

Lites, B. W., Shine, R. A., and Hansen, E. G., 1979, "Line Formation in the Solar Chromosphere. II. An Optically Thick Region of the Chromosphere-Corona Transition Region Observed with OSO-8," to appear in Astrophys. J., Feb. 15, 1980.

November, L., J. Toomre, K. Gebbie, G. W. Simon, E. C. Bruner, E. G. Chipman, B. W. Lites, F. Q. Orrall, R. A. Shine, R. G. Athay, O. R. White, "Supergranulation Velocity Fields Observed in the Solar Transition Region with OSO-8," presented at the 148th Meeting of the American Astronomical Society (Haverford, PA), B.A.A.S., 8, 311, 1976.

November, L., J. Toomre, K. Gebbie, G. Simon, "Vertical and Horizontal Components of Supergranulation Velocity Fields Observed with OSO-8," presented at the 150th meeting of the American Astronomical Society (Atlanta, GA), B.A.A.S., 9, 337, 1977.

The following papers using data from the University of Colorado experiment were published in Proceedings of the November 7-10, 1977 OSO-8 Workshop, Hansen and Schaffner, eds.

<u>Paper</u>	<u>Page</u>
"Partial Coherent Scattering in the Wings of Lyman $\alpha$ ", D. Roussel-Dupré, G. S. Basri . . . . .	29
"A Chromospheric Model Generator", R. A. Shine . . . . .	36
"Formation of the O I Lines in the Solar Chromosphere", D. Skelton, R. A. Shine (Abstract) . . . . .	55
"Overlapping Emission Peaks in the Solar C I Multiplets at $\lambda 1560$ and $\lambda 1657$ ", R. A. Shine, B. W. Lites, E. G. Chipman (Abstract) . . . . .	56
"Line Formation in the Solar Chromosphere: I. The C II Resonance Lines Observed with OSO-8", B. W. Lites, R. A. Shine, E. G. Chipman (Abstract) . . . . .	57
"The Establishment of a Facular Model from the Photosphere to the Corona: Preliminary Results on C IV Lines", S. Dumont, Z. Mouradian, J. C. Pecker, E. G. Chipman . . . . .	183
"The Cell-Network Structure of the Transition Zone", E. C. Bruner, Jr., R. W. P. McWhirter (Abstract) . . . . .	191
"Ultraviolet Brightenings in Active Regions as Observed From OSO-8", B. W. Lites, E. R. Hansen (Abstract) . . . . .	217
"Mass Motions in Impulsive Flare-like Brightenings as Observed by OSO-8", E. C. Bruner, Jr., B. W. Lites, D. W. Datlowe . . . . .	218
"Chromospheric Oscillations in Si II: Power and Phase Spectra", R. G. Athay, O. R. White . . . . .	344

"OSO-8 Observations of Frequency Dependent Phase Velocities of Waves in the Chromosphere", E. G. Chipman . . . . .	357
"Limb Broadening of Quiet Sun Transition Zone Lines from OSO-8 Observations", R. Roussel-Dupré, M. H. Francis, D. E. Billings . . . . .	442
"Supergranulation Velocity Fields", L. J. November, J. Toomre, K. B. Gebbie, G. W. Simon (Abstract) . . . . .	451
"OSO-8 Experiment Operations", E. R. Hansen . . . . .	452
"Computer Codes for OSO-8 Pointing and Planning", E. G. Chipman .	464
"LASP/OSO-8 Calibration", G. Rottman (Abstract) . . . . .	469

## APPENDIX III

### UNIVERSITY OF COLORADO ENGINEERING REPORT: OSO-SLIT MALFUNCTION

#### A. SLIT MECHANISM DESCRIPTION

The slit mechanism consists of a 48 position stepper motor mechanically connected to a circular 48 position slit wheel. The control to the stepper motor is a four phase winding with internal communication. The electrical control for the motor is a dual motor driver (DMD). The DMD steps the motor by sequentially switching each phase to ground. To assure proper stepping, the phase adjacent to the last phase energized must be enabled. One may thus step the mechanism forward or reverse by enabling the phase on either side of the last energized phase. A single command is used to step the motor one step forward. To step the wheel reverse, three fast step forward commands are rapidly issued. This can be done under "Jr" control.

The dual motor driver consists of redundant systems of control step counters, and into a 4PDT switching relay to the motor windings.

The control for the motor drivers initializes and synchronizes each ring counter during turn-on of logic power. The control also disables drive to the motor with a .05 Hz clock. Drive is reenabled with a step pulse.

The step counters are J-K flip-flops connected to count through four states. The counter is then decoded and coupled to the optical isolators. These provide the electrical isolation and drive to the Darlington switching transistors for sequentially switching.

The redundant output from the Darlington transistors is connected to the motor by a 4PDT relay which is commandable to either position by pulse commands from the engineering logic unit.

#### B. CHRONOLOGY OF PROBLEMS AND SOLUTIONS

- August 5, 1975: The slit mechanism mechanically stuck between two slit openings and could not be stepped in either direction.
- August 12, 1975: After cooling the instrument by about 3°C, the slit was stepped to a 20 arcsec slit.
- March 4, 1976: The slit was commanded to make one reverse step and stuck mechanically. Three individual forward step commands were issued, and the slit opened on a 20 arcsec slit. This new slit was determined to be two positions in the reverse direction from the original. Thus, the slit stuck when moved in the forward direction

and freed when moved reverse, indicating a mechanical wedging effect.

- March 14, 1977: An electrical problem caused the Colorado instrument to draw an increased 200 m Amp of power.
- March 16, 1977: This power increase heated the instrument about 3°C.
- March 20, 1977: The wavelength drive motor was not able to step.
- March 24, 1977: After cooling the instrument by 2.5°C, the wavelength drive operated successfully.
- March 24 - April 1, 1977: Many diagnostic electronic tests were run. It was determined that all electronic subsystems, except the focus, wavelength and slit subassemblies, were nominal. The focus assembly was not thoroughly tested. The wavelength drive operated nominally using Side A of the motor driver electronics, but Side B drew increased current, indicating an electrical problem in these unused electronics. The slit subassembly was not thoroughly tested at this time because of its known mechanical problems. However, the instrument temperatures of March 14, 1977, showed that the temperatures nearest the slit assembly increased prior to other other temperatures, indicating that the increased power originated in the slit electronics.

### C. SLIT TESTS AND PROCEDURES

From July 31 to August 5, 1977 another attempt was made to move the slit and/or determine the electrical problems associated with this assembly. In preparation for this operation, the instrument temperatures were lowered by selecting times when the spacecraft days were shortest and the spacecraft was furthest from the sun, by orienting the spacecraft to a pitch angle of  $< 0^\circ$ , by pointing the instrument optical axis to deep space prior to critical procedures, and by disabling instrument subassemblies.

From July 31 to August 2, 1977 several small raster mode experiments were executed at the top and bottom solar limbs. These data were reduced to determine both the positions of the limbs and the coalignment between the CU and CNRS instruments. These benchmark values would later be used to evaluate any slit motion.

August 3, QUI Orbit 11678: The slit was enabled and stepped once reverse (this was accomplished with three rapid slit step commands). The reverse step command caused the motor winding in the reverse direction to be enabled for about 15 seconds. During this time the spectrometer counts decreased to zero. After the

- (b) A motor winding is always in the enabled state.
- (c) It is likely that the 200 mA of extra current observed on March 14, 1977, was caused by this problem.

Three failure explanations were possible:

1. A non-redundant motor winding is shorted. This would cause a current increase of 180 mA or greater, depending on where in the winding (and how much resistance) the short occurred.

2. A two-point failure where a component failure in one side of the motor driver electronics enabled current to one motor continuously, and a second mechanical or electrical failure prohibiting the relay to switch from one motor driver to the other. If this is valid, it would be possible to fix the problem by causing the relay to trip to the redundant motor driver.

3. A failure in components on both sides of the motor driver electronics causing a motor winding to be enabled continuously, no matter which set of electronics was used.

August 4, MIL 11700: Since it was unlikely that both redundant motor drivers would have ring counters in the same phase, it was possible to test for failure 3. The slit was enabled and four rapid step commands were issued under Jr. control, reenabling the motor winding corresponding to the present slit position. No current increase was observed, verifying previous tests. The relay was then commanded to switch to the redundant electronics and four rapid steps commanded. Again there was no current increase. Thus, failure 3 was for the most part ruled out.

In the hopes that failure 2 was correct, several attempts were made to switch the relay. If the relay switched, the current would decrease by at least 150 mA.

ORR 11694: The relay was commanded to switch 9 times with no drop in current.

AGO 11706: Colorado 28V regulated power was disabled. This might cause a possible shorted transistor in the relay electronics to come up in a correct state.

QUI 11708: Colorado 28V power was reenabled with no drop in current. The relay was commanded to switch 8 times, first to the backup electronics and then to the normal electronics, again with no drop in current.

ORR 116709: Bursts of 97 relay switch commands were issued to switch alternately between sides. There was no decrease in current.

motor winding disabled, the counts returned to the original level (or perhaps a level somewhat higher as seen in the following figure).

August 3, MIL 11682 and ROS 11683: Raster mode experiments were repeated at the top and bottom limbs to determine if the slit had moved. The results clearly showed that neither the limb positions nor the coalignment with CNRS had changed and that the slit had not moved.

Four conditions could cause the observed anomaly:

1. A motor winding was shorted on with the ring counter in phase. The step command caused two adjacent windings to be enabled for 15 seconds during which the slit was positioned between the two poles.

2. No motor winding shorted, but the ring counter was out of phase. The step command caused the slit to move into the mechanical "wedge" which prevented it from stepping. When the motor winding power was released, the slit was no longer held against the wedge and moved to the nearest magnetic detent position.

3. A motor winding was shorted on, and the ring counter was out of phase. This would be similar to case 1.

4. No motor winding was shorted, but the ring counter was out of phase. The slit was originally at one phase, and a motor winding two positions away was enabled. While the second motor winding was enabled, the slit moved toward the new position but the weak magnetic pull could not pull the slit wheel to a new position.

August 4, QUI 11693: A procedure was set up to determine which of the four explanations was valid.

The slit was enabled and stepped once reverse. A current increase of 150 mA was measured with no loss in spectrometer counts. These results eliminated explanation No. 3 since in that situation we would have seen a current increase of less than 60 mA.

The slit was then rapidly stepped twice forward. There was no increase in current and no loss of data counts. Therefore, cases 2 and 4 were invalid since we should have seen a current increase with both these explanations. Case 1, where a motor winding was shorted on, explained the slit problem.

The following information was used to further diagnose the observed failure:

(a) Both sides of the redundant slit motor driver electronics draw the same amount of current.

ORR 116710: Groups of commands, to "buzz" the relay at about 10 Hz, were uplinked. These groups were issued several times, first ending on the normal side and then the backup side. There was no decrease in current.

#### D. CONCLUSION

We were unable to step the slit wheel since one motor winding is continuously enabled. This situation could be caused by a single point failure of a short in one of the non-redundant motor windings or by a two-level problem of both a relay failure and a component failure in the electronic motor driver.

## Appendix V

## Contents of Words in Experiment and Record Headers

EXPERIMENT HEADER FORMAT  
(FINAL DATA)

WORD NUMBER	WORD TYPE*	CONTENTS
1	I	Tape ID: Colorado = 1; Paris = 2; Raw data = 3
2	I	Control of SEAS: Colorado = 1; Paris = 0
3	I	Tape type: always = 3 for Final data tape
4	I	Number of minor frames with sync errors
5	I	2* number of minor frames of fill (erroneously added twice each minor frame by TSTM1 and PACK)
6	I	Not used (always zero)
7	I	Orbit number (calculated)
8-9	I,I	S/C Clock -- 32 bit integer number
10	I	Time at start of experiment -- day
11	I	Time at start of experiment -- hour
12	I	Time at start of experiment -- minute
13	I	Time at start of experiment -- second
14	I	Time at end of experiment -- day
15	I	Time at end of experiment -- hour
16	I	Time at end of experiment -- minute
17	I	Time at end of experiment -- second
18	I	S/C mode from "Junior"
19	I	Never filled (always zero)
20	I	Number of logical records in experiment
21	I	Logical record size (in 16 bit words)
22	I	Code for ground station ID: (B means octal value) 24B=Rosman; 10B=Santiago; 20B=Joburg; 26B=Tananarive; 147B=Ascension; 45B=Hawaii; 107B=Mila; 25B=Ororal; 154B=Madrid, 5B=Quito; 143B=Bermuda; 0=Unknown

\* I = integer; R = real; B = BCD

## EXPERIMENT HEADER FORMAT -- FINAL DATA

WORD NUMBER	WORD TYPE	CONTENTS
23	I	Right ascension of spin axis $\times 10^2$ (deg)
24	I	Declination of spin axis $\times 10^2$ (deg)
25	I	Roll angle $\times 10^2$ (deg)
26	I	Pitch angle $\times 10^2$ (deg)
27	I	Commanded azimuth $\times 10^2$ (arc min)
28	I	Commanded elevation $\times 10^2$ (arc min)
29	I	Actual azimuth $\times 10^2$ (arc min)
30	I	Actual elevation $\times 10^2$ (arc min)
31	I	Component of velocity on sun line -- start of experiment ( $\times 10^2$ for FDPLÖT)
32	I	Component of velocity on sun line - end of experiment ( $\times 10^2$ for FDPLÖT)
33	I	Always = 0
34	I	Always = 0
35-44	I	Coefficients used to correct wavelength 5 floating point numbers
45		Not used
46-48		Used by FDPLÖT only for file name (in PDP code, Radix-50)
49	I	Year
50-59		Blank
60	I	Experiment type
61	I	Experiment serial number
62	I	Experiment category (type of solar region)
63	I	Detector: T = 2; G = 3
64	I	Filter
65	I	Starting slit position

## EXPERIMENT HEADER FORMAT -- FINAL DATA

WORD NUMBER	WORD TYPE	CONTENTS
66	I	Slit length (arc sec)
67-68	I,I	Starting wavelength drive step number (32 bits)
69-70	I,I	Ending wavelength drive step number (32 bits)
71	I	Starting wavelength x 10 (angstroms)
72	I	Ending wavelength x 10 (angstroms)
73-74	R	Gate time (sec)
75-76	R	Time interval between observations (sec)
77	I	Gate time, clock and sync
78	I	Number of observations on a line
79	I	Number of wavelength drive steps between observations
80-81	R	Number of angstroms between observations
82	I	Number of repeats over scan range
83	I	Number of disc positions
84	I	Number of slit positions
85	I	Number of steps between slit positions
86		Not used
87		Not used
88	I	Wavelength correction, from calibration experiment
89	I	Number of repeats of experiment before calibration
90	I	Slit position of max or min
91	I	Max or min flag: max = 1; min = 0
92-93	I,I	Wavelength drive position of max or min (32-bit step number)

## EXPERIMENT HEADER FORMAT -- FINAT DATA

WORD NUMBER	WORD TYPE	CONTENTS
94	I	Wavelength drive position of max or min x 10 (angstroms)
95	I	Flag for experiment completeness: 0=no messages, 1=beginning message read, 2=end but no beginning message; 3-both beginning and end=complete experiment
96	I	React experiment: 0=normal; 1=react
97	I	Experiment sequence number
98	I	ith dimension of data array
99	I	jth dimension of data array
100	I	Spectral order: 1=1st order; 2=second order
101	I	First logical record on output tape file
102	I	Last logical record on output tape file
103	I	Wavelength drive stuck on null -- number of times during experiment set-up
104	I	Wavelength drive stuck off null -- number of times during experiment set-up
105-118	I , I	(Maximum seven) Starting and ending wavelengths of additional lines (in multiple line experiments) (angstroms and times 10 angstroms in FD PLOT)
119-132	R	Gate times of additional lines
133	I	Total wavelength drive errors
134-137	R	Starting and ending wavelength (angstroms)
138-149		Not used
150	I	Actual S/C mode
151	I	Modified type (1 to 48)
152	I	GMT year
153	I	Flag for min/max experiment: 1=minimum; 2=maximum
154	I	Total number of wavelength errors during experiment set-up and execution

## EXPERIMENT HEADER FORMAT -- FINAL DATA

WORD NUMBER	WORD TYPE	CONTENTS
155	B	CDC display code file name left shifted, zero filled
156	I	2*number of minor frames read in (to current half of Major Frame) (error caused twice correct number added by SPEC and TSTM1)
157	I	Flag that S/C mode changed during experiment: 0=no change; 1=did change
158	I	Number of Orbital Geometry data entries (jth index) Array size=13 by j; maximum j=150
159	I	Number of Status Monitor entries (jth index), Array size = 70 by j; max. j = 50
160	I	Number of pointing coordinates entries (jth index) array size = 5 by j; max j = 225
161	I	Number of single-bit errors
162	I	Number of multi-bit errors
163	I	Day of last sunrise
164	I	Hour of last sunrise
165	I	Second of last sunrise
166	I	Second of last sunrise
167	I	Day of last sunset
168	I	Hour of last sunset
169	I	Minute of last sunset
170	I	Second of last sunset
171	I	Number of GSFC fill words written by Goddard into DMA
172	I	FINSCI program version number (starting at 0)
173	I	Wavelength drive offset flag: 0=absolute; 1=offset
174-5	R	Wavelength drive offset value (calculated, angstroms)

EXPERIMENT HEADER FORMAT -- FINAL DATA

WORD NUMBER	WORD TYPE	CONTENTS
176	I	Time in GMT milliseconds when S/C mode changed (to closest Major Frame)
177	I	Job run-tape creation date (mmddyy) (Main program)
178		Not used
179-80	R	Wheel spin rate (radians/degree)
197	I	Old experiment sequence number (0 if unchanged)

ORIGINAL PAGE IS  
OF POOR QUALITY

LOGICAL RECORD HEADER FORMAT  
(FINAL DATA)

WORD NUMBER	WORD* TYPE	CONTENTS
1	I	144444B Logical record ID
2	I	144444B
3	I	ith dimension of logical data array to follow
4	I	jth dimension of logical data array to follow
5	I	Variable type: 64000B = integer; 74000 = floating point
6-12		Not used
13	I	Repetition number (logical record number)
14	I	Commanded azimuth $\times 10^2$ (arc min)
15	I	Commanded elevation $\times 10^2$ (arc min)
16	I	New slit position
17	I	Starting wavelength $\times 10$ (angstroms)
18	I	Ending wavelength $\times 10$ (angstroms)
19-20	R	Number angstroms between observations
21	I	Time at start of logical record -- day
22	I	Time at start of logical record -- hour
23	I	Time at start of logical record -- minute
24	I	Time at start of logical record -- second
25	I	High voltage detector being used
26	I	Overflow indicator ( <u>1</u> = overflow; 0 = no overflow)
27	I	Junior error -- count and location
28		Never filled (always 0)
29		Not used
30		Never filled (always =0)

\* I = integer; R = real

## LOGICAL RECORD HEADER FORMAT -- FINAL DATA

WORD NUMBER	WORD TYPE	CONTENTS
31	I	Number of times wavelength drive stuck on null during logical record
32	I	Position of data element just before error flagged in word above: high 8 bits = row number, low 8 bits = column number
33-34	R	Seconds of elapsed time between 'on null' error and next data element
35	I	Position of second error
36-37	R	Time of second error
38	I	Position of third error
39-40	R	Time of third error
41	I	Number of times wavelength drive stuck 'off null' during logical record
42	I	Position of first error
43-44	R	Time of first error
45	I	Position of second error
46-47	R	Time of second error
48	I	Position of third error
49-50	R	Time of third error
51-55	I	Absolute temperature 1-5
56	I	Junior memory I module temperature
57	I	Junior power supply temperature
58	I	Junior memory medium temperature
59-75	I	Differential temperatures #1-17
76	I	Missing data flag: 0 = no missing data; >0 = number of times data missing

LOGICAL RECORD HEADER FORMAT -- FINAL DATA

WORD NUMBER	WORD TYPE	CONTENTS
77	I	Experiment type number (1-23)
78-87	R	Coefficients used for wavelength calibration
88-94	I	Offset wavelengths of additional lines (in multiple line scan experiments). A 16 bit offset from beginning of previous scan in wavelength drive step positions
95-108	R	Starting and ending of additional lines x 10 (angstroms)
109-122	R	Gate times of additional lines in seconds
123-136	R	Time interval between observations for additional lines in seconds
137-143	I	Gate time, clock and sync for additional lines
144-147		Floating point starting and ending wavelength in angstroms
148-149		Not used
150	I	True spacecraft mode
151	I	Calculated actual azimuth (arc min) x 10 <sup>2</sup> For raster experiments only
152	I	Calculated actual elevation (arc min) x 10 <sup>2</sup> For raster experiments only
153	I	Junior recorded spacecraft mode
154	I	Number of GSFC fill words in logical record
155	R	Time of last sunrise (decimal days)
193-256	I	Junior memory dump

APPENDIX VII  
 SORTED FINAL DATA TAPES  
 CONTENTS, RANGE, AND CATALOG #'s

Tape Name	Catalog #	# Files	Start Date Yr Day Hr	End Date Yr Day Hr	Range of File Numbers
LB-1	#1	146	75-271-12	75-365-22	4159-7301
LB-2	#2	137	76-002-16	76-082-15	7336-9505
LB-3	#3	30	76-082-17	76-099-07	9507-10053
LB-4	#4	73	76-100-10	76-142-07	10078-11285
LB-5	#5	51	76-154-11	76-174-04	11526-11962
LB-6	#6	122	76-174-23	76-217-09	11982-12968
LB-7	#7	62	76-228-22	76-287-09	13299-15193
LB-8	#8	55	76-313-19	76-354-21	15786-16672
LB-9	#9	65	76-356-00	77-033-08	16710-17404
LB-10	#10	181	77-327-02	78-069-21	22133-23400
LB-11	#11	5	78-071-14	78-072-03	23463-23476
LB-12	#12	22	78-073-02	78-098-08	23481-24297
LB-13	#13	9	78-161-11	78-164-15	26321-26440
LB-14	#14	4	78-164-20	78-166-01	26446-26479
LB-15	#15	93	78-166-15	78-273-09	26492-29919

Tape Name	Catalog #	# Files	Start Date Yr Day Hr	End Date Yr Day Hr	Range of File Numbers
X-1	#100	201	75-179-07	76-099-18	264-10056
X-2	#101	293	76-100-04	76-255-03	10069-14124
X-3	#102	109	76-305-01	77-049-21	3900-17732
X-4	#103	3	78-118-09	78-203-02	24929-27943
R-1	#21	383	75-174-11	75-309-05	1-5880
R-2	#22	436	75-321-10	76-082-08	6172-9498
R-3	#23	377	76-134-15	76-264-21	10869-14412
R-4	#24	97	76-265-21	76-299-16	14428-15454
R-5	#25	299	76-301-11	77-005-11	15495-16950
R-6	#26	51	77-012-11	77-037-09	17077-17469
R-7	#27	240	77-256-15	78-175-10	21604-26635
M-1	#16	500	75-174-14	76-099-08	4-10054
M-2	#17	404	76-100-03	76-297-07	10068-15406
M-3	#18	125	76-300-11	77-048-04	15471-17690
M-4	#19	292	77-114-15	78-129-09	19090-25371
M-5	#20	161	78-131-21	78-261-06	25421-29627

Tape Name	Catalog #	# Files	Start Date Yr Day Hr	End Date Yr Day Hr	Range of File Numbers
SS-1	#28	570	75-174-17	75-199-21	14-1246
SS-2	#29	616	75-200-00	75-217-21	1247-2626
SS-3	#30	423	75-225-14	75-259-20	2655-3681
SS-4	#31	481	75-260-00	75-269-07	3684-30697
SS-5	#32	476	75-290-00	75-329-21	4953-6404
SS-6	#33	490	75-330-01	76-057-17	6409-8914
SS-7	#34	212	76-061-13	76-099-17	9034-10055
SS-8	#35	340	76-100-02	76-179-16	10067-12094
SS-9	#36	559	76-180-10	76-244-13	12112-13886
SS-10	#37	449	76-245-01	76-299-22	13897-15462
SS-11	#38	376	76-309-00	76-334-21	15461-16315
SS-12	#39	293	76-334-22	77-027-03	16315-17306
SS-13	#40	36	77-033-11	77-049-21	17406-17733
SS-14	#41	287	77-242-22	78-048-05	21506-23002
SS-15	#42	483	78-051-11	78-099-22	23014-24377
SS-16	#43	546	78-099-22	78-159-21	24379-26259
SS-17	#44	515	78-159-21	78-208-05	26259-28120
SS-18	#45	473	78-209-20	78-273-17	28156-29927

Tape Name	Catalog #	# Files	Start Date Yr Day Hr	End Date Yr Day Hr	Range of File Numbers
S-1	#46	244	75-174-13	75-209-22	2-2060
S-2	#47	298	75-210-03	75-249-19	2073-3357
S-3	#48	347	75-249-21	75-269-17	3359-4016
S-4	#49	432	75-269-22	75-289-20	4030-4949
S-5	#50	416	75-290-00	75-319-21	4952-6144
S-6	#51	178	75-319-23	75-349-21	6145-6883
S-7	#52	194	75-350-00	76-009-22	6887-7494
S-8	#53	307	76-010-10	76-034-21	7512-8256
S-9A	#54	101	76-035-06	76-042-18	8268-8537
S-9B	#55	96	76-042-20	76-049-21	8539-8713
S-10	#56	131	76-049-22	76-059-20	8714-8997
S-11	#57	149	76-061-10	76-079-13	9031-9442
S-12	#58	233	76-080-08	76-099-22	9464-10059
S-13	#59	134	76-099-22	76-114-15	10059-10372
S-14	#60	207	76-114-17	76-134-10	10374-10866
S-15	#61	386	76-137-10	76-148-07	10925-11416
S-16	#62	178	76-148-10	76-174-20	11418-11980
S-17	#63	151	76-174-22	76-204-21	11981-12732
S-18	#64	151	76-204-23	76-231-16	12733-13360
S-19	#65	144	76-235-09	76-264-20	13480-14411
S-20	#66	223	76-265-15	76-288-14	14424-15225
S-21	#67	65	76-294-10	76-299-21	15332-15459
S-22	#68	154	76-300-00	76-329-21	15463-16150
S-23	#69	177	76-329-23	76-354-19	16153-16670
S-24	#70	111	76-355-02	77-029-12	16676-17340
S-25	#71	100	77-029-23	77-044-23	17347-17615
S-26	#72	66	77-045-00	77-049-16	17617-17728
S-27	#73	220	77-114-15	77-279-17	19089-21852
S-28	#74	161	77-281-04	77-311-19	21860-22082
S-29	#75	124	77-325-12	77-358-05	22123-22443
S-30	#76	50	78-006-10	78-019-22	22444-22634
S-31	#77	126	78-019-22	78-049-00	22634-23010

S-32	#78	117	78-054-10	78-079-23	23074-23686
S-33	#79	441	78-080-10	78-129-22	23694-25379
S-34	#80	203	78-130-09	78-154-17	25386-25996
S-35	#81	460	78-154-21	78-209-05	26000-28139
S-36	#82	171	78-209-06	78-229-21	28140-28856
S-37	#83	355	78-229-23	78-273-15	28858-29925

ORIGINAL PAGE IS  
OF POOR QUALITY

Tape Name	Catalog #	# Files	Start Date Yr Day Hr	End Date Yr Day Hr	Range of File Numbers
V-1	#84	216	75-176-09	75-269-06	61-30695
V-2	#85	122	75-289-21	75-319-08	4950-6121
V-3	#86	110	75-320-08	75-349-21	6151-6885
V-4	#87	35	75-350-00	76-004-21	6888-7377
V-5	#88	189	76-004-22	76-058-01	7379-8921
V-6	#89	111	76-061-19	76-097-22	9044-10014
V-7	#90	76	76-100-01	76-129-20	10066-10702
V-8	#91	105	76-130-13	76-167-22	10745-11804
V-9	#92	139	76-177-05	76-210-05	12042-12823
V-10	#93	161	76-217-20	76-264-23	12979-14414
V-11	#94	130	76-265-00	76-299-21	14415-15460
V-12	#95	122	76-300-19	76-357-02	15478-16731
V-13	#96	82	77-023-17	77-049-22	17213-17734
V-14	#97	240	77-345-19	78-089-05	22303-23926
V-15	#98	327	78-090-05	78-206-07	23955-28081
V-16	#99	259	78-217-21	78-273-15	28289-29926

ORIGINAL PAGE IS  
OF POOR QUALITY